Polynuclear Rhodium Complexes with Dinucleating PNNP Ligand: Dynamic and Diverse M···M Interactions in $[(\mu\text{-X})Rh_2(PNNP)(CO)_2]^{n+}$ and $[(\mu_4\text{-X})Rh_4(PNNP)_2(CO)_4]^{n+}$ [X = H, O, C≡C−R, R−C≡C−R, C≡C, CH=CH_2, SMe_2; *n* = 0, 1: PNNP = 3,5-bis(diphenylphosphinomethyl)pyrazolato]

Shukichi Tanaka, Christian Dubs, Akiko Inagaki, and Munetaka Akita*

Chemical Resources Laboratory, Tokyo Institute of Technology, R1-27, 4259 Nagatsuta, Midori-ku, Yokohama 226-8503, Japan

Received July 26, 2004

The dirhodium-tetracarbonyl complex with the PNNP ligand, $[Rh_2(PNNP)(CO)_4]BF_4$, **1**·BF_4 [PNNP = 3,5-bis(diphenylphosphinomethyl)pyrazolato], serves as a precursor for the active species $[Rh_2(PNNP)(CO)_2]^+$, **A**, with *cis*-divacant coordination sites, which can accommodate a donor species with up to four donor electrons. Interaction of **1**·BF_4 with Li−C≡C−R, Li−CH=CH_2, PPN[$M(CO)_n$], CN−Cy, SMe_2, and Et−C≡C−Et leads to the formation of the corresponding dinuclear adducts $[(X)Rh_2(PNNP)(CO)_2]^{n+}(BF_4)_n$ [X/*n* = μ-η^1:η^2-C≡C−R/0 (**2**), μ-η^1:η^2-CH=CH_2/0 (**3**), μ-$Co(CO)_4$/0 (**4a**), μ-$Mn(CO)_5$/0 (**4b**), (η^1-C≡N−Cy)$_2$/1 (**5**·BF_4), μ-η^1:η^1-SMe_2/1 (**6**·BF_4), μ-η^2:η^2-Et−C≡C−Et/1 (**7**·BF_4)], respectively. Selective replacement of the inner CO ligands *trans* to the P atoms is verified by spectroscopic and crystallographic characterizations of the adducts. The μ-acetylide (**2**) and μ-vinyl complexes (**3**) show dynamic behavior via the conventional windshield wiper motion of the unsaturated hydrocarbyl ligand. Systematic structural analysis of a series of the μ-acetylide complexes **2** (R = H, $SiMe_3$, *n*-Bu, Ph, *p*-tol) reveals three typical conformations for the $Rh_2(PNNP)(CO)_2$ backbone: C_s- (type I), C_2- (type II), and C_{2v}-symmetrical ones (type III). On the other hand, interaction of **1**·BF_4 with 1-alkyne, hydrosilanes, and hydroxo anion produces tetranuclear adducts resulting from 1 (donor):2 $[Rh_2(PNNP)(CO)_2]$ coupling reactions. The μ_4-$\eta^1(C_\alpha)$:$\eta^2(C_\alpha{\equiv}C_\beta)$-acetylide complexes, $[(\mu_4\text{-C}{\equiv}\text{C−R})Rh_4(PNNP)_2(CO)_4]BF_4$, **8**·$BF_4$, consisting of an acyclic, folded Z-shaped Rh_4 linkage are fluxional via a combination of windshield wiper-like motions between the wingtip Rh centers and between the wingtip and hinge Rh centers, which involve reversible M−M bond scission and recombination processes. The ethynyl complex **8a**·BF_4 (R = H) is readily deprotonated by the action of a base to give the μ_4-dicarbide complex (μ-η^1:η^1:η^2:η^2-C≡C)$Rh_4(PNNP)(CO)_4$, **9**, via cleavage of three Rh−Rh bonds, and this process is reversed upon protonation of **9** with HBF_4. The reaction of **1**·BF_4 with hydrosilanes and hydroxo anion furnishes the isostructural tetranuclear complexes $[(\mu_4\text{-X})Rh_4(PNNP)(CO)_4]^{n+}(BF_4)_n$ [X/*n* = H/1 (**10**·BF_4), O/0 (**11**)], in which the four Rh atoms arranged in a tetrahedral array are connected by the μ_4-bridging ligand (X), as characterized by X-ray crystallography. The tetranuclear structures are retained mainly by Rh−X interactions even in the case of the electron-deficient hydride complex **10**·BF_4 with 58 valence electrons (cf. 64e for a coordinatively saturated species), where the filled, spherically distributed 1s orbital of the hydride ligand interacts with the four Rh centers arranged in a tetrahedral array. Depending on the size of the bridging ligand X, the structure of the tetranuclear complexes varies from the encapsulated structure (**10**·BF_4 and **11**) to the one with a folded Z-shaped metal linkage (**8**·BF_4). The present study reveals (i) the high reactivity (electrophilicity) of the active species **A** with *cis*-divacant coordination sites, (ii) M−M bonds being not always essential for a polynuclear system, (iii) dynamic behavior via reversible M−M bond cleavage and recombination processes, and (iv) flexible coordination properties of the $Rh_2(PNNP)$ system.

Introduction

Polynuclear transition metal complexes are expected to display unique chemical reactivity based on a cooperative action of the metal centers.[1] Many polynuclear organometallic complexes are supported by metal−metal bonds, which are regarded as a key structural motif of so-called cluster compounds. On the other hand, little attention has been paid to polynuclear transition metal organometallics not supported by metal−metal bonds, in contrast to relevant inorganic systems such as polyoxometalates and bioinorganic model complexes, which have been studied extensively.[2]

10.1021/om049427v CCC: $30.25
Publication on Web 12/01/2004

Scheme 1

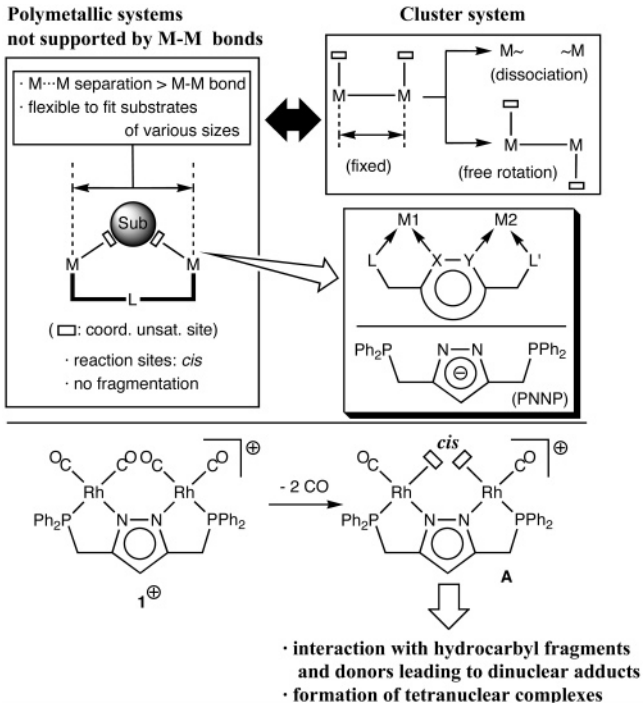

We have been interested in the latter type of polynuclear organometallic systems and initiated the research on those containing the PNNP ligand [3,5-bis(diphenylphosphinomethyl)pyrazolato] developed twenty years ago by Bosnich (Scheme 1).[3] Doubly donor-tethered heteroaromatics such as pyrazole and pyridazine derivatives are versatile dinucleating ligands with two chelating coordination sites,[2c] and the PNNP ligand belongs to this class of ligand. It is expected that this type of ligand (i) holds the two metal centers bridged by it at a distance longer than M−M bonding interaction and (ii) is so flexible as to fit substrates of various sizes by adjusting the M···M separation. Furthermore, (iii) regio- and stereochemistry of other ancillary ligands as well as coordinatively unsaturated sites can be controlled. For example, if two coordinatively unsaturated sites can be generated on *cis* sites (e.g., **A** in Scheme 1), they may cooperate to interact with or activate a substrate in a concerted manner. In addition, (iv) the chelating coordination suppresses fragmentation of the dinuclear structure. These features are in contrast to those of M−M bonded systems, where (i) the M−M distance is fixed, (ii) M−M bonds may be cleaved during a reaction course, and (iii) rotation around the M−M bond may lead to a *trans* conformation, which is not suitable for a concerted interaction.

Herein we describe results of the study on polynuclear rhodium complexes containing the PNNP ligand.[4] Bosnich reported the synthesis and some basic reactivity of Rh− and Ir−PNNP complexes including catalytic activity for olefin hydrogenation.[3] They also indicated that the labile dirhodium tetracarbonyl complex, $[Rh_2(PNNP)(CO)_4]BF_4$ (**1**·BF_4), served as a precursor for the *cis*-divacant active species **A**, but detailed reaction features of the intriguing dinuclear system with organic substrates were left to be studied. This contribution is divided into three parts, which deal with (I) dinuclear complexes formed by interaction of **1**·BF_4 with hydrocarbyl fragments and donor molecules, (II) unique tetranuclear systems resulting from dimerization of the Rh_2(PNNP) fragment, and (III) coordination features of the PNNP ligand.

Results and Discussion

I. Dinuclear Complexes. A variety of dinuclear adducts were obtained upon treatment of **1**·BF_4 with hydrocarbyl fragments and donor molecules.

Dinuclear *μ*-Acetylide Complexes 2. (i) Synthesis. Treatment of **1**·BF_4 with lithium acetylide in THF readily produced neutral dinuclear complexes with substituted alkynyl groups **2b**−**e** as yellow crystals, and the parent ethynyl complex **2a** was obtained via desilylation of the $SiMe_3$ derivative **2b** in THF in the presence of a catalytic amount of NBu_4·F (Scheme 2). Reaction of **1**·BF_4 with 1-alkyne gave tetranuclear complexes **8**·BF_4 as described below (see section II).

Scheme 2

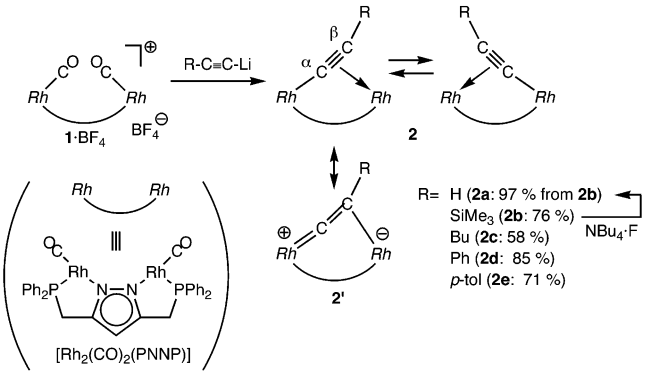

(ii) Spectroscopic Characterization. Spectroscopic data for **2** are summarized in Table 1. The dinuclear *μ*-acetylide complexes **2** show dynamic behavior, which is interpreted in terms of the conventional windshield wiper motion mechanism as characterized by low-temperature ^1H, ^{31}P, and ^{13}C NMR measurements. As a typical example, NMR charts for the $SiMe_3$ derivative **2b**·BF_4 are shown in Figure 1. The single doublet ^1H and ^{31}P NMR signals for the CH_2P moiety (δ_H 3.79 (J_{H-P} = 10.2 Hz; δ_P 49.7 (J_{P-Rh} = 142 Hz)). observed at room temperature separate into two doublets at low temperatures (below −60 °C), and in accord with this change, coupling of the acetylide $\delta_C(C_\alpha)$ signal changes from a triplet-of-triplets (J_{C-Rh} = 54 Hz, J_{C-P} = 27 Hz; coupling with two equivalent RhP fragments) to a doublet-of-

(1) Abel, E. W.; Stone, F. G. A.; Wilkinson, G. *Comprehensive Organometallic Chemistry II*; Pergamon: Oxford, 1995; Vols. 3−10. Dyson, P. J.; McIndoe, J. S. *Transition Metal Carbonyl Cluster Chemistry*; Gordon and Breach Science: Amsterdam, 2000. Shriver, D. F.; Kaesz, H. D.; Adams, R. D. *The Chemistry of Metal Cluster Complexes*; VCH: New York, 1990.

(2) (a) See, for example, special issue for polyoxometalates: *Chem. Rev.* **1998**, *98*, 1−388. (b) Yamase, T: Pope, M. T. *Polyoxometalate Chemistry for Nano-Composite Design (Nanostructure Science and Technology)*; Kluwer Academic: New York; 2002. (c) Gavrilova, A. L.; Bosnich, B. *Chem. Rev.* **2004**, *104*, 349.

(3) (a) Schenk, T. G.; Downs, J. M.; Milne, C. R. C.; Mackenzie, P. B.; Boucher, H.; Whelan, J.; Bosnich, B. *Inorg. Chem.* **1985**, *24*, 2334. (b) Schenk, T. G.; Milne, C. R. C.; Sawyer, J. F.; Bosnich, B. *Inorg. Chem.* **1985**, *24*, 2338. See also: (c) Bosnich, B. *Inorg. Chem.* **1999**, *38*, 2554.

(4) Part of the results were reported as preliminary communications. Tanaka, S.; Akita, M. *Angew. Chem., Int. Ed.* **2001**, *40*, 2865. Tanaka, S.; Dubs, C.; Inagaki, A.; Akita, M. *Organometallics* **2004**, *23*, 317.

Table 1. Selected Spectroscopic Data for $[(\mu\text{-X})Rh_2(PNNP)(CO)_2]^{n+}$ and $[(\mu_4\text{-X})Rh_4(PNNP)_2(CO)_4]^{n+}$ [a]

		^{1}H NMR (δ_H)			^{13}C{^{1}H} NMR (δ_C)				^{31}P NMR	IR (cm^{-1}/KBr)	
complex	X	X	CH_2P[b]	pz[c]	X	CH_2P[d]	pz[e]	CO[f]	(δ_P)[g]	ν_{CO}	ν_X
2a[h]	C≡C−H	4.12 (1H, m)	3.85 (10.8)	6.03	87.2 (dd, 233,[i] 18.4,[j] 9.2,[k] C_β) 121.1 (tt, 57.9,[j] 28.0,[k] C_α)	35.4 (27.6)	99.0 (11.1) 153.7 (9.2, 3.7)	194.7 (64.3, 14.8)	48.5 (139.9)	1976, 1964	3235 1859
2b[h]	C≡C−$SiMe_3$	0.41 (9H, s)	3.79 (10.2)	6.03	0.94 (s, $SiMe_3$), 102.7 (tt, 18.4,[j] 9.2,[k] C_β) 147.3 (tt, 55.1,[j] 24.8,[k] C_α)	33.7 (25.7)	98.0 (11.9) 152.4 (7.3, 3.7)	193.6 (65.2, 13.8)	49.7 (142)	1966, 1948	1909
2c[h]	C≡C−Bu	*l*	3.80 (10.9)	6.01	106.6 (m, C≡C), 107.4 (br, C≡C)[l]	35.1 (25.7)	98.9 (11.9) 153.1 (9.2, 3.6)	195.3 (66.2, 14.7)	49.8 (141.0)	1972, 1944	*m*
2d[h]	C≡C−Ph	*a*	3.77 (10.6)	5.98	*n*				51.0 (142.0)	1975, 1963	*m*
2e[h]	C≡C-tol	2.37 (3H, s)[a]	3.80 (10.6)	6.04	21.5 (s, Me), 105.7 (br, C≡C), 117.5 (br, C≡C)[a]	34.5 (27.5)	99.1 (11.9) 153.1 (9.2, 3.7)	194.6 (67.6, 13. 8)	51.1 (143.1)	1975, 1966	*m*
3[o]	CH═CH_2	5.67 (1H)[p] 6.52 (1H)[p]	3.60 (dd, 16.5, 7.3) 3.95 (dd, 16.5, 13.5)	6.05					49.9 (131.5)	1972	
4a[h]	$Co(CO)_4$		3.72 (11.6)	5.99	210.4 (br, Co−CO)	33.9 (26)	100.7 (12), 154.3 (9, 4)	192.1 (64.3, 12.9)	44.0 (172.6)	1972, 1911, 1856	
4b[h]	$Mn(CO)_5$		3.81 (11.2)	6.02	226.1 (s, Mn−CO)	34.7 (27.5)	100.5 (11.9) 154.4 (br. d, 7.3)	193.5 (66.1, 12.9)	42.6 (171.5)	2024, 1997, 1968, 1915, 1877, 1831	
5·BF_4[o]	$(NC-Cy)_2$	*q*	3.70 (dd, 17.0, 5.4, 2H) 4.2−4.3 (m, 2H)	6.33	*q*	30.9 (27.6)	102.3 (11.0) 156.5 (br. d, 7.3)	191.0 (65.3, 15.6)	49.4 (129.4)	1989	2187
6·BF_4[o]	SMe_2	3.48 (6H, s, Me)	4.25 (11.6)	6.30	32.5 (s, Me)	35.4 (30.7)	101.3 (12.5) 154.2 (m)	191.5 (66.9, 15.1)	49.0 (d, 159.9)	1979	
7·BF_4[o]	3-hexyne	1.60 (t, 7.3, 6H, Me) 3.49 (q, 7.3, 4H, CH_2)	4.28 (11.6)	6.28	15.4 (s, Me) 25.8 (s, CH_2) 76.9 (br, ≡C)	35.4 (29.4)	101.3 (11.9) 154.4 (br)	191.0 (67.0, 13.8)	45.3 (164.1)	1988	
8a·BF_4[h]	C≡C−H	6.82 (1H, s)	3.79 (11.2)	6.13	93.8 (brd, 237,[i] C_β) *r*	33.8 (29.3)	99.9 (11.9) 153.4 (9.2, 3.7)	190.5 (61.5, 15.6)	54.6 (179.9)	1977	
8b·BF_4[h]	C≡C−$SiMe_3$	0.26 (9H, s)	3.81 (11.6)	6.19	3.64 (s, $SiMe_3$), 77.6 (br, C_α), 116.8 (br, C_β)	32.9 (29.4)	100.0 (11.9) 152.9 (8.2, 4.6)	191.1 (62.4, 14.7)	55.1 (183.0)	1982	
8c·BF_4[h]	C≡C−Bu	*s*	3.79 (11.2)	6.19	77.4 (br, C_α), 118.3 (br, C_β),	33.5 (29.4)	100.1 (11.9) 153.5 (9.2, 3.7)	191.2 (62.4, 14.8)	56.7 (184.0)	1973	

complex	X	^{1}H NMR (δ_H) X	CH_2P^b	pz^c	^{13}C{^{1}H} NMR (δ_C) X	CH_2P^d	pz^e	CO^f	^{31}P NMR (δ_P)^g	IR (cm^{-1}/KBr) ν_{CO}	ν_X
8d·BF_4[o]	C≡C−Ph	*a*	4.01 (11.6)	6.27	77.0 (br, C_α), 112.6 (br, C_β)[a]	33.6 (29.3)	100.9 (11.9) 154.5 (8.3, 4.8)	192.0 (62.4, 14.7)	59.9 (181.0)	1978	
8e·BF_4[h]	C≡C-tol	2.39 (3H, s)	3.79 (10.9)	6.18	22.0 (s, Me), 75.5 (qq, 25.0,[i] 14.0[k]) 112.6 (br, C_β)[a]	33.9 (29.3)	100.2 (12.0) 153.7 (9.1, 3.7)	191.2 (62.4, 14.7)	56.3 (184.0)	1976	
9[h]	C≡C		3.78 (10.9)	5.99	119.5 (tt, 33.0,[j] 17.2,[k] C_2)	35.2 (27.5)	98.9 (11.9) 153.4 (11.0, 3.7)	194.0 (64.3, 14.7)	48.2 (151.5)	1963	
10[h]	μ_4-H	−9.39 (qq, 31.2,[l] 13.6)[a]	3.68 (10.0)	6.24		31.8 (29)	100.3 (12) 155.4 (9, 4)	192.4 (62, 11)	63.7 (200)	1983	
11[h]	μ_4-O		3.82 (10.9)	5.93					50.3 (161.0, 3.6[v])	1955	

[a] Observed at 200 Hz (^{1}H), 100 MHz (^{13}C), 81 MHz (^{31}P). Aromatic signals are shown in the Experimental Section. [b] Doublet (J_{H-P}). [c] Signals for the hydrogen atom at the 4-position of the pyrazolyl ring; singlet. [d] Doublet (J_{C-P}). [e] δ_C ~100 for 4-pz; triplet (J_{C-P}); δ_C ~150 for 3,5-pz: doublet of doublets (J_{C-P}). [f] Doublet of doublets: J_{C-Rh} = ~60 Hz; J_{C-P} = ~15 Hz. [g] Doublet (J_{P-Rh}). [h] NMR in CD_2Cl_2. [i] J_{C-H}. [j] J_{C-Rh}. [k] J_{C-P}. [l] **2c**: δ_H 0.99 (3H, t, J_{H-P} = 7.3 Hz, Me), 1.62, 1.85, 2.87 (2H × 3, m × 3, CH_2); δ_C 14.0 (s, Me), 22.4, 25.9, 34.3 (s, $(CH_2)_3$). [m] Not located. [n] Owing to the low solubility in organic solvents, ^{13}C NMR data could not be obtained. [o] NMR in acetone-d_6. [p] δ_H 5.72 (ddt, J = 21.0, 6.0, 1.4 Hz), 6.52 (apparent sextet, J = 5.8 Hz); the other vinyl proton signal could not be located owing to overlap with the aromatic signals. [q] δ_H 1.3−2.1 (m, 20H, Cy-CH_2), 4.2−4.3 (m, 4H, CN*CH*); δ_C 23.6, 25.4, 33.0, 55.9. [r] C_α signal could not be located. [s] δ_H 0.77 (3H, t, J = 7.6 Hz, Me), 1.30, 1.92 (2H × 2, m × 2, $(CH_2)_2$), 3.44 (2H, t, J = 6.4 Hz, ≡C−CH_2); δ_C 13.8 (s, Me), 22.5, 32.4, 34.8 (s, CH_2). [t] J_{H-Rh}. [u] J_{H-P}. [v] Triplet.

doublets (J_{C-Rh} = 104 Hz, J_{C-P} = 47 Hz). The J_{C-Rh} and J_{C-P} values observed at room temperature should be averaged values of those with the σ- and π-bonded RhP units observed at −80 °C, and therefore, coupling constants with the π-bonded unit at −80 °C are estimated to be J_{C-Rh} = ~4 Hz and J_{C-P} = ~7 Hz, suggesting an interaction of C_α with the σ-bonded Rh atom much stronger than that with the π-bonded one.

The ^{1}H NMR signal for the ethynyl hydrogen atom in **2a** is located at δ_H 4.12, and the α- and β-carbon signals are unequivocally assigned on the basis of the J_{C-H} coupling constants [at rt: $\delta_C(C_\beta)$ 87.2 (dd, J_{C-H} = 233 Hz, J_{C-Rh} = 18.4 Hz, J_{C-P} = 9.2 Hz), $\delta_C(C_\alpha)$ 121.1 (tt, J_{C-Rh} = 57.9 Hz, J_{C-P} = 28.0 Hz; J_{C-H} coupling for C_α is obscured by the J_{C-Rh} and J_{C-P} couplings)]. The large J_{C-H} value for the C_β signal clearly indicates its sp-character. The acetylide carbon signals for the $SiMe_3$ derivative **2b** are also located at $\delta_C(C_\beta)$ 102.7 (tt, J_{C-Rh} = 18.4 Hz, J_{C-P} = 9.2 Hz) and $\delta_C(C_\alpha)$ 147.3 (tt, J_{C-Rh} = 55.1 Hz, J_{C-P} = 24.8 Hz). The deshielding of the $\delta_C(C_\alpha)$ signal could be attributed to contribution of a vinylidene resonance structure (**2′**; Scheme 2). Because, however, the difference in $\delta_C(C_\alpha)$ and $\delta_C(C_\beta)$ is not so large and the $\delta_C(C_\alpha)$ signals are located in much higher field compared with those of typical vinylidene complexes (δ_C >250),[5] the contribution of **2′** is not significant, as is consistent with the X-ray results (see below). The $\delta_C(C_\alpha)$ and $\delta_C(C_\beta)$ signals for **2c**,**e** appear in a narrow range as broad multiplets due to weak couplings [δ_C 106.6, 107.4 (**2c**); 105.7, 117.5 (**2e**)] and are tentatively assigned following the trends observed for **2a**,**b**.[6]

The neutral acetylide complexes **2** show two ν_{CO} vibrations in the region of 1950−1980 cm^{-1}, which are lower in energies than those of the starting cationic species **1**·BF_4 [2086, 2019, 1977 cm^{-1} (KBr)].

(iii) Crystallographic Characterization. All dinuclear μ-acetylide complexes obtained (**2a**−**e**) are characterized by X-ray crystallography. Selected structural parameters are summarized in Table 2, and ORTEP views are shown in Figure 2.

The acetylide ligand bridges the two Rh centers in a μ-η^1:η^2-fashion as usually observed for dinuclear μ-acetylide complexes.[7] The Rh coordination planes are virtually planar except for **2d** (β_2 = 24.8°), as judged by the small dihedral angles (β: 2−9°; see Scheme 3) made by the P1−Rh1−N1 and C1−Rh1−C01 planes (β_1 for Rh1) and the P2−Rh2−N2 and M−Rh2−C02 planes (β_2 for Rh2; M: midpoint of C≡C). The C≡C lengths (1.20−1.25 Å) are comparable to those in previously reported related complexes.[8] The C≡C−R groups are η^1-bonded to Rh1 and η^2-bonded to Rh2, and accordingly, the C1−Rh1 distances are substantially shorter than the C1−Rh2 distances, as is consistent with the different coupling constants with the two Rh centers mentioned above. Despite the support by the dinucleating PNNP ligand, the differences in the Rh−C distances (Δ_1: 0.2−0.3 Å)

(5) Bruce, M. I. *Chem. Rev.* **1991**, *91*, 197. Bruce, M. I.; Swincer, A. G. *Adv. Organomet. Chem.* **1983**, *22*, 59. See also: Bruce, M. I. *Chem. Rev.* **1998**, *98*, 2797.

(6) Low solubility of the Ph derivative **2d** hampered obtaining a ^{13}C NMR spectrum of a sufficient S/N ratio.

(7) Lotz, S.; van Rooyen, P. H.; Meyer, R. *Adv. Organomet. Chem.* **1995**, *37*, 219.

(8) Hartley, F. R.; Patai, S.; Rappoport, Z. *The Chemistry of the Metal−Carbon Bond*; Wiley: New York, 1982. See also references therein.

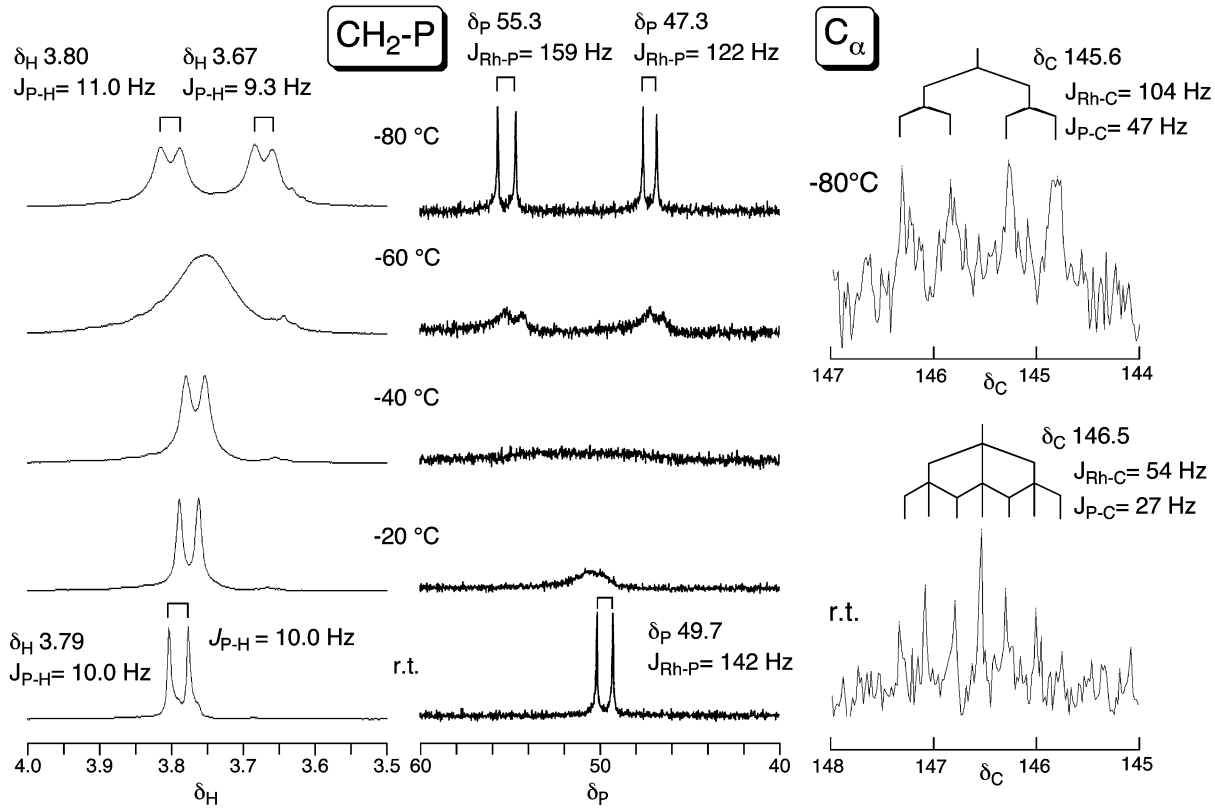

Figure 1. Variable-temperature ^{1}H (400 MHz), ^{31}P (162 MHz), and ^{13}C NMR spectra (100 MHz) for **2b** observed in CD_2Cl_2.

Table 2. Selected Structural Parameters for (μ-C≡C−R)Rh$_2$(PNNP)(CO)$_2$, 2^a

complex	**2a**	**2b**^{b}		**2c**	**2d**	**2e**
R	H	$SiMe_3$		n-Bu	Ph	tol
C1−C2	1.215(3)	1.23(1)	1.215(9)	1.20(2)	1.252(8)	1.205(5)
Rh1−C1	2.030(2)	2.028(7)	2.020(6)	2.06(1)	2.098(5)	2.061(3)
Rh2−C1	2.399(2)	2.395(7)	2.399(8)	2.358(9)	2.319(5)	2.338(2)
Rh2−C2	2.294(2)	2.314(7)	2.321(7)	2.31(1)	2.313(6)	2.388(3)
Rh1−P1	2.2825(6)	2.297(2)	2.287(2)	2.276(3)	2.251(2)	2.2768(8)
Rh2−P2	2.2210(6)	2.234(2)	2.229(2)	2.253(3)	2.220(2)	2.2405(7)
Rh1−N1	2.028(2)	2.016(5)	2.028(5)	2.025(7)	2.029(5)	2.030(2)
Rh2−N2	2.061(2)	2.061(5)	2.078(4)	2.057(7)	2.052(5)	2.066(2)
Rh1−C01	1.819(3)	1.827(7)	1.807(7)	1.81(1)	1.815(6)	1.826(3)
Rh2−C02	1.820(3)	1.815(7)	1.833(6)	1.83(1)	1.824(7)	1.825(3)
C01−O01	1.147(4)	1.152(8)	1.164(9)	1.15(1)	1.159(8)	1.145(5)
C02−O02	1.150(4)	1.145(9)	1.127(8)	1.14(1)	1.153(9)	1.149(4)
Rh1···Rh2	3.7718(2)	3.7939(9)	3.7892(9)	3.6588(9)	3.6882(5)	3.6169(4)
Rh1−C1−C2	172(1)	167.6(6)	167.1(7)	172(1)	156.5(5)	168.7(3)
C1−C2−R	128	149.7(6)	150.6(7)	161(1)	164.3(6)	164.3(3)
C1−Rh2−C2	29.7(4)	30.2(2)	29.8(2)	29.7(4)	31.4(2)	29.5(1)
Δ_1	0.369	0.367	0.379	0.30	0.221	0.277
Δ_2	0.105	0.081	0.078	0.05	0.006	−0.050
θ_1	18.2(4)	18.7(1)	20.4(1)	38.8(2)	51.8(1)	40.27(6)
α_1	−10.55(8)	−19.2(2)	−19.5(2)	25.1(4)	−1.6(2)	20.9(1)
α_2	12.81(9)	21.5(2)	23.1(2)	24.1(3)	2.4(2)	34.0(1)
β_1	5.2	6.8	7.7	3.0	9.6	3.9
β_2	9.4	5.6	6.7	5.3	24.8	2.1
γ_{12}	14.8(2)	21.5(6)	22.0(6)	−1(1)	9.8(7)	−0.9(4)

^{a} Interatomic distances in Å and bond angles in deg. Δ_1 (in Å): d(C1−Rh1) − d(C1−Rh2). Δ_2 (in Å): d(Rh2−C1) − d(Rh2−C2). θ_1 (in deg): dihedral angle between the planes defined by Rh2−P2−N2−C02 and Rh2−C1−C2. For $\alpha - \gamma$ (in deg), see Scheme 3. β_2 (in deg): dihedral angle between the P2−Rh2−N2 and M-Rh2−C02 planes (M: midpoint of C1−C2). ^{b} Two independent molecules.

and the Rh···Rh separations (3.6−3.8 Å) are similar to those in dinuclear μ-acetylide complexes without any additional bridging interaction [e.g., (μ-η^1:η^2-C≡C−R)-{Fe(η^5-C_5Me_5)$(CO)_2$}$_2$]$^+BF_4^-$: Δ_1 = 0.308 Å (R = H), 0.223 Å (R = Ph); M···M = 4.038(1) Å (R = H), 4.012(1) Å (R = Ph)].[9] As for the η^2-coordination to Rh2, differences in the Rh2−C1,C2 distances (Δ_2) are rather small (0.105 to −0.050 Å), indicating a virtually symmetrical η^2-coordination with a minor contribution of the unsymmetrical vinylidene form **2′** (Scheme 2).

A difference is found for the η^2-coordination geometry of the C≡C moiety with respect to the Rh2 coordination plane. The dihedral angles (θ_1) made by the Rh2

(9) Akita, M.; Terada, M.; Oyama, S.; Moro-oka, Y. *Organometallics* **1990**, *9*, 816.

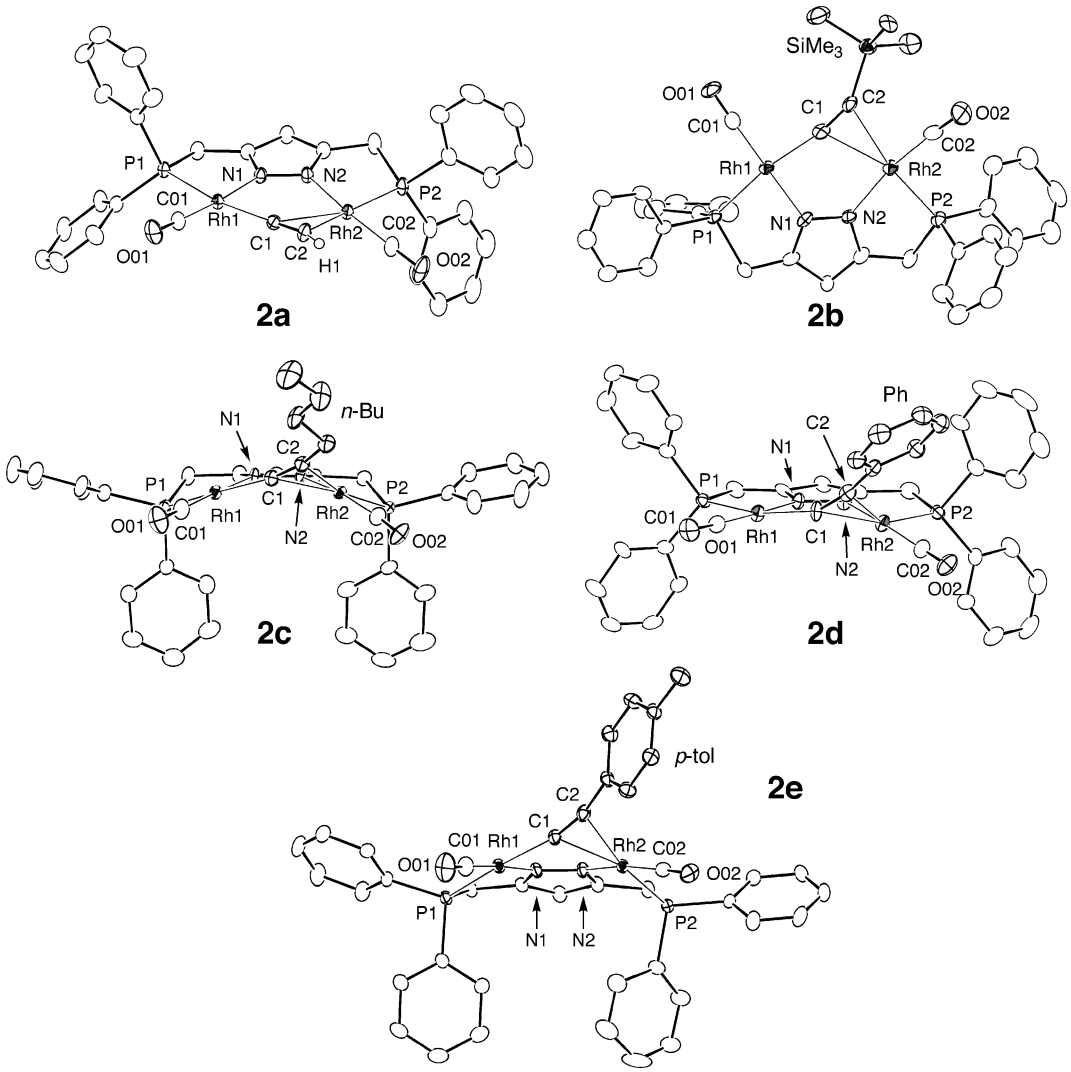

Figure 2. Molecular structures for **2a**−**e** drawn with thermal ellipsoids at the 30% probability level. For **2b** one of two independent molecules is shown.

Scheme 3

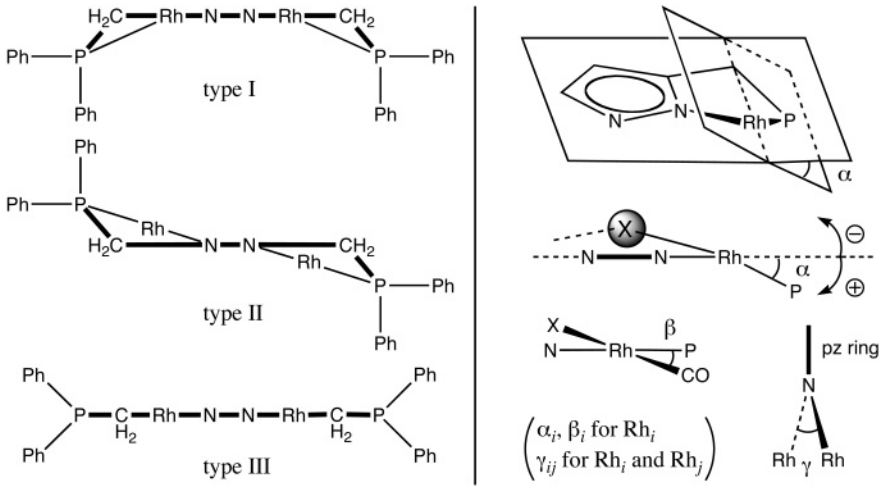

coordination plane (Rh2−P2−N2−C02) and the (C≡C)-Rh2 plane (Rh2−C1−C2) are variable in the range 18−52°. As the size of the substituent (R) becomes larger, the C≡C part tends to be arranged perpendicular (twisted) with respect to the Rh2 coordination plane. It is reported that, in the case of square-planar η^2-alkene or -alkyne complexes of d^8-metals, the parallel and perpendicular arrangements are not so different in energy, and the orientation of the alkene and alkyne ligand is dominated by steric repulsions with other ancillary ligands.[10] In the case of **2**, steric repulsion

(10) Albright, T. A.; Hoffmann, R.; Thibault, J. C.; Thorn, D. L. *J. Am. Chem. Soc.* **1979**, *101*, 3801.

between the acetylide substituent and the CO ligand attached to Rh2 (C02−O02) should cause the deformation from an in-plane arrangement to a perpendicular form, although the Rh1−C1 σ-bond forces an in-plane conformation. The steric repulsion is also released by twisting the Rh−N−N−Rh linkage (γ: Scheme 3), in particular, for **2b** with the bulky $SiMe_3$ group [$\gamma \sim 22° > 14-1°$ (**2a**,**c**−**e**)].

In contrast to the similar (μ-C≡C−R)Rh_2 core structures in **2**, the structures of the $Rh_2(PNNP)(CO)_2$ backbone, in particular, the arrangement of the phenyl rings attached to the P atoms, are considerably different and can be classified into three groups: apparently C_s- (type I: **2c**,**e**), C_2- (type II: **2a**,**b**), and C_{2v}-symmetrical structures (type III: **2d**) (Scheme 3).[11] The three structural types can be characterized on the basis of the conformation of the five-membered azaphospharhodacyclopentenes fused to the central pyrazolyl ring. The azaphospharhodacyclopentene in the $Rh_2(PNNP)$ part may adopt an envelope-like conformation in a manner similar to cyclopentene,[12] where the sp^3-hybridized phosphorus atom is bent out of the virtually planar Rh−N=C−CH_2 part containing the C=N functional group, and the extent of the bending can be estimated by the dihedral angle between the Rh−P−CH_2 plane and the Rh−N=C−CH_2 plane (α_1 for Rh1 and α_2 for Rh2; Scheme 3). The ± sign refers to the direction of the puckering of the metallacycle with respect to the orientation of the μ-acetylide ligand. A positive value corresponds to the situation where the metallacycle is puckered in the direction opposite the projection of the acetylide, whereas a negative value refers to the conformation where the metallacycle is puckered in the same direction as the projection of the acetylide. On the basis of the α_1 and α_2 values, the three structural types are characterized as follows: type I (α_1, $\alpha_2 > 0$), type II ($\alpha_1 < 0$, $\alpha_2 > 0$), and type III (α_1, $\alpha_2 \sim 0$). In the case of type I complexes (**2c**,**e**), the two metallacycles are folded away from the projection of the acetylide ligand. As a result, two phenyl groups are projected in the downward axial direction and the other two phenyl groups occupy the equatorial positions, leading to a C_s-symmetrical backbone structure. Because the strain may be relieved by the puckering of the metallacycles, no significant distortion is observed for the Rh−N−N−Rh moiety, as judged by the very small γ values, indicating a planar conformation for the central Rh_2 moiety. Contrastingly, in the case of type II complexes (**2a**,**b**), the two metallacycles are puckered in the opposite directions; the Rh2-metallacycle is puckered downward as observed for type I complexes, whereas the Rh1-metallacycle is puckered upward. As a result, the Rh−N−N−Rh linkage (γ) is twisted to a considerable extent to lead to the C_2-symmetrical $Rh_2(PNNP)(CO)_2$ backbone, which causes projection of two phenyl groups to the opposite axial directions. The type III complex (**2d**) contains essentially planar metallacycles, which cause projection of the four phenyl groups in the diagonal directions, leading to the apparent C_{2v}-symmetrical $Rh_2(PNNP)(CO)_2$ backbone. The extent of twisting of the Rh−N−N−Rh linkage (γ) is in the middle of those of the other two categories, but the Rh2 coordination plane is most distorted, as is evident from the largest θ_1 and β_2 values.

Thus the various conformations observed for **2** are a result of the steric repulsion between the μ-acetylide ligand and the $Rh_2(PNNP)(CO)_2$ backbone (in particular, CO2−O02) under the constraint of the Rh···Rh separation being ca. 3.7 Å. The steric repulsion is released by a combination of (i) puckering of the azaphospharhodacyclopentenes (α), (ii) distortion of the Rh coordination structure from a square-planar geometry (β), (iii) twisting of the Rh−N−N−Rh linkage (γ), and (iv) twisting of the C≡C moiety with respect to Rh2 (θ_1). The conformation of the Ph rings should also be influenced by intermolecular interactions, including $\pi-\pi$ stacking and C−H π-interaction,[13] because the aryl derivatives **2d**,**e** with essentially the same steric and electronic demands adopt considerably different backbone structures.

Taking into account the conformations observed for **2**, their dynamic behavior can be discussed in detail (Scheme 4). Averaging of all four CH_2P signals (^1H NMR) at the first exchange limit could be explained by a combination of two intermediates, **B** and **C**. The windshield wiper motion proceeds via the C_{2v}-symmetrical intermediate **B** (process *a*), and through this process, all four CH_2P protons become equivalent at room temperature. The decoalescence of the CH_2P signals of **2b** at low temperatures mentioned above (Figure 1a: single doublet → two doublets) is consistent with the situation, where process *a* is frozen out, but flipping of the acetylide ligand above and below the PNNP plane (process *b*) is still ongoing ($H_a = H_b \neq H_c = H_d$), because (i) at the slow exchange limit of the two processes, all four CH_2P protons should be inequivalent and (ii) slowing process *a* causes the appearance of two ^{31}P NMR signals at low temperatures (Figure 1), which is the case (cf. one signal for slowing process *b*). This result reveals that process *a* is higher in energy than process *b*. The acetylide ligand in **B** loses the π-interaction in contrast to that in **C**, in which the μ-η^1:η^2-coordination of the acetylide ligand is retained.

Vinylation and Metalation of 1·BF_4. The successful synthesis of the μ-acetylide complexes **2** was followed by attempts at introduction of sp^2- and sp^3-hybridized hydrocarbyl fragments. While an unstable μ-vinyl complex **3** was obtained and characterized as described below, attempted alkylation (e.g., with n-BuLi) resulted in intractable mixtures of products. Then metalation of **1**·BF_4 with $[Co(CO)_4]^-$ and $[Mn(CO)_5]^-$, which are isolobal [14] with the alkyl anion, was examined.

(i) μ-Vinyl Complex [(μ-CH=CH_2)Rh_2(PNNP)-$(CO)_2$], 3. Reaction of **1**·BF_4 with vinyllithium generated by treatment of $Sn(CH{=}CH_2)_4$ with n-BuLi gave the yellow product **3** quantitatively (Scheme 5). It was essential to use a halide-free alkyllithium reagent.[15] Otherwise **1**·BF_4 readily reacted with the halide anion present in the reagent to give the μ-halo complex (μ-X)-

(11) Conformation of chelating ligands has been discussed in detail for many complexes. See, for example, for asymmetric catalysis: Brown, J. M.; Chalonaer, P. A. In *Homogeneous Catalysis with Metal Phosphine Complexes*; Pignolet, L. H., Ed.; Plenum: New York, 1983.

(12) McMurry, J. *Organic Chemistry*, 6th ed.; Brooks/Cole: Belmont, 2003.

(13) Jorgensen, W. L.; Severance, D. L. . *J. Am. Chem. Soc.* **1990**, *112*, 4768.

(14) Hoffmann, R. *Angew. Chem., Int. Ed.* **1982**, *21*, 711. Albright, T. A.; Burdett, J. K.; Whangbo, M.-H. *Orbital Interactions in Chemistry*; Wiley: New York, 1985.

(15) Juenge, E. C.; Seyferth, D. *J. Org. Chem.* **1961**, *26*, 563.

Scheme 4

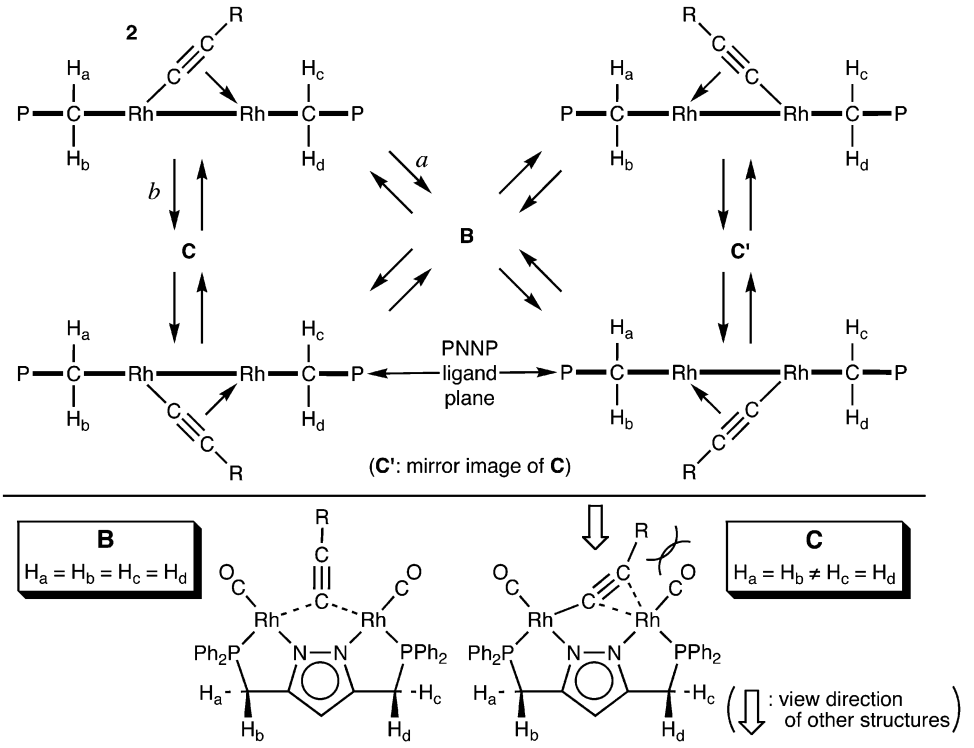

Scheme 5

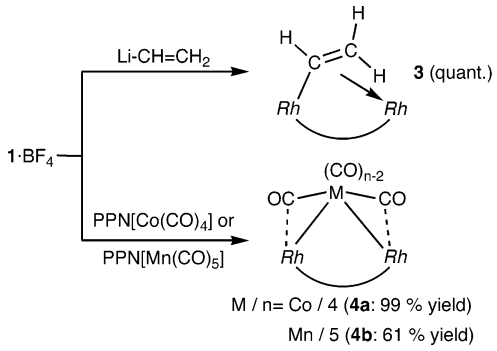

Rh_2(PNNP)$(CO)_2$ preferentially. Low solubility of **3** in organic solvents and decomposition upon attempted dissolution in CH_2Cl_2 and acetone hampered further purification of **3**, which was characterized by NMR (^{1}H, ^{31}P) and IR.

The vinyl-methylene ^{1}H NMR signals are located at δ_H 5.72 (ddt, J = 21.0, 6.0, 1.4 Hz) and 6.52 (apparently sextet, J = 5.8 Hz), which appear as complicated signals owing to coupling not only with each other but also with the Rh and P nuclei, but the vinyl-methine proton signal should overlap with the aromatic proton signals. At room temperature only one ^{31}P NMR signal is observed, suggesting the occurrence of a dynamic behavior. Because, however, the CH_2P ^{1}H NMR signals appear as two separate dd signals with geminal CH_2 coupling [δ_H 3.95 (J_{H-H} = 16.5 Hz, J_{H-P} = 13.5 Hz), 3.60 (J_{H-H} = 16.5 Hz, J_{H-P} = 7.3 Hz)] even at room temperature (at the first exchange limit), a windshield wiper motion should be responsible for the dynamic process and flipping of the vinyl ligand (similar to process *b* in Scheme 4) is not working.

(ii) Trinuclear Rh_2M Complexes with a Bent Rh−M−Rh Array, (PNNP)$Rh_2M(CO)_n$ [M/*n* = Co/6 (4a), Mn/7 (4b)]. Reaction of **1**·BF_4 with metalates PPN[$M(CO)_n$] readily produced trinuclear adducts **4a** and **4b** (Scheme 5). Composition of the adducts (PNNP)-$Rh_2M(CO)_{n+2}$ [M/n = Co/4 (**4a**), Mn/5 (**4b**)] is supported by FD-MS data, and semibridging CO vibrations (∼1850 cm^{-1}) suggest formation of metal−metal bonds. X-ray crystallography (Figure 3 and Table 3) reveals the trinuclear structures consisting of an open Rh−M−Rh

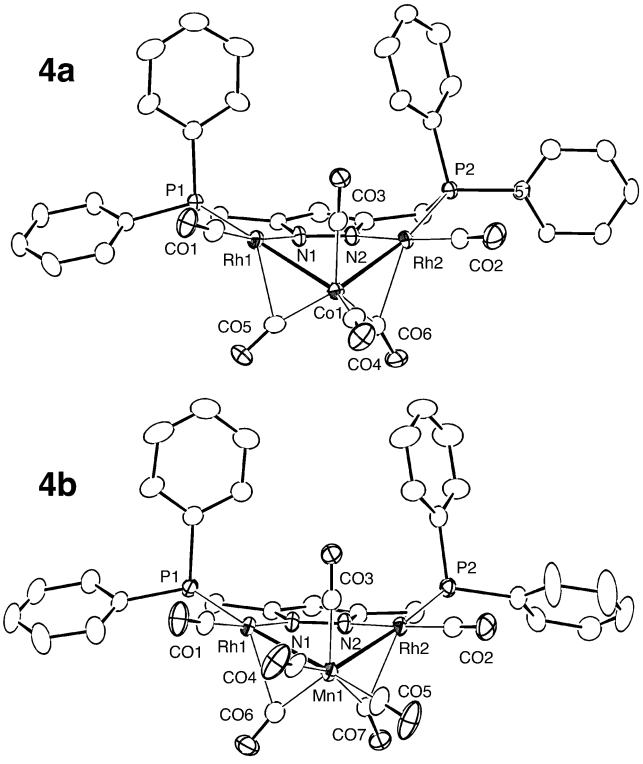

Figure 3. Molecular structures for **4a** and **4b** drawn with thermal ellipsoids at the 30% probability level.

Table 3. Selected Structural Parameters for (PNNP)$Rh_2M(CO)_{n+2}$, 4[a]

	4a	**4b**
$M(CO)_n$	$Co(CO)_4$	$Mn(CO)_5$
Rh1−M	2.6688(8)	2.747(1)
Rh2−M	2.647(1)	2.7381(7)
Rh1−P1	2.255(1)	2.262(2)
Rh2−P2	2.252(2)	2.282(1)
Rh1−N1	2.070(5)	2.070(4)
Rh1−CO	1.840(8) (C1)	1.835(6) (C1)
	2.345(6) (C5)	2.407(7) (C6)
Rh2−N2	2.057(5)	2.068(6)
Rh2−CO	1.842(7) (C2)	1.847(9) (C2)
	2.308(6) (C6)	2.255(5) (C7)
M−CO	1.790(6) (C3)	1.848(6) (C3)
	1.778(8) (C4)	1.825(7) (C4)
	1.794(6) (C5)	1.814(9) (C5)
	1.807(6) (C6)	1.853(7) (C6)
		1.884(6) (C7)
C−O	1.12−1.15	1.13−1.17
M−C−O (μ-CO)	163.4(6) (CO5)	166.4(7) (CO6)
	162.2(6) (CO6)	160.7(4) (CO7)
Rh−C−O (μ-CO)	117.4(4) (CO5)	114.4(6) (CO6)
	118.8(5) (CO6)	117.0(4) (CO7)
M−C−Rh	79.1(2) (CO5)	79.1(2) (CO6)
	79.0(2) (CO6)	82.3(2) (CO7)
Rh1···Rh2	3.8131(6)	3.8846(5)
Rh1−M−Rh2	91.67(3)	90.19(3)

[a] Interatomic distances in Å and bond angles in deg.

Scheme 6

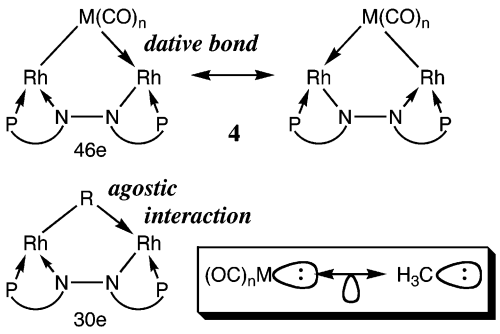

linkage with bent angles of 91.67(3)° (**4a**) and 90.19(3)° (**4b**) and the Rh···Rh separations of 3.8131(6) Å (**4b**) and 3.8846(5) Å (**4b**), which are much longer than a Rh−Rh bond (<3.3 Å; see below). The two complexes are virtually isostructural except the number of η^1-CO ligands attached to M and the bulky $M(CO)_n$ fragments lead to type I conformation for the PNNP ligands. The semibridging CO ligands weakly interact with the Rh centers, as judged by (i) the Co−C−O angles (160−166°) larger than the Rh···C−O angles (114−119°) and (ii) the Rh···C separations (>2.2 Å) much longer than the Co−C lengths (∼1.8 Å). Accordingly, ^{13}C NMR signals for the CO ligands attached to Rh and M are observed separately, and the $M(CO)_n$ moieties show single broad resonances owing to site exchange between the terminal and semibridging CO ligands reaching the fast exchange limit at ambient temperature. It is also notable that the symmetrical structures of **4** result from resonance hybridization of two canonical structures with a dative M→Rh interaction,[16] which leads to an electron-precise 46e configuration [18e (M) + 16e (square-planar Rh) × 2 − 2e (Co−Rh bond) × 2 = 46e] (Scheme 6). Although an alkyl complex cannot be obtained, introduction of the isolobal $M(CO)_n$ fragments gives **4** with a dative M−Rh interaction, which would correspond to an agostic interaction[17] in a putative alkyl complex.

Scheme 7

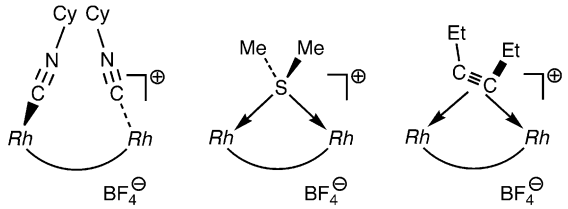

5·BF_4 (95 % yield) **6**·BF_4 (65 % yield) **7**·BF_4

Introduction of Neutral Donor Molecules into the Rh_2(PNNP) System. In addition to the reactions of **1**·BF_4 with anionic species described above, interaction with neutral donors was also examined, and the reaction products are shown in Scheme 7.

Reaction of **1**·BF_4 with cyclohexylisonitrile readily afforded the substituted product **5** in quantitative yield. An IR spectrum of **5** contains a $\nu_{C\equiv N}$ vibration (2187 cm^{-1}) in addition to a $\nu_{C\equiv O}$ band (1989 cm^{-1}), and FD-MS data are consistent with the composition. ^1H NMR signals for the CH_2P moiety appear as two dd signals [2H × 2; J_{H-P}, J_{H-H}(geminal)], in contrast to the single doublet signal (4H; J_{H-P}) observed for **1**·BF_4, while a symmetrical structure is suggested by the single ^{31}P NMR signal. These NMR features are consistent with a structure resulting from replacement of the inner CO ligands *trans* to P in **1**·BF_4. The sterically congested situation brought about by introduction of the bulky R−NC ligands should be relieved by taking a C_2-symmetrical twisted conformation to make the CH_2P protons diastereotopic, and the bulky R−NC ligands should hinder switching of their sites, which should lead to NMR features consistent with a C_{2v}-symmetrical structure. On the other hand, replacement of the outer CO ligands *trans* to N would not affect the situation of the central $Rh_2(CO)_2$ part leading to a single doublet CH_2P signal (^1H NMR) as observed for **1**·BF_4, but this is not the case, as is evident from the NMR data. It is therefore concluded that the inner CO ligands are more labile than the outer CO ligands, as mentioned in the Introduction, and this should be attributed to the *trans* effect of the P atom, which is stronger than that of the N atom of the pyrazolyl moiety.[18] Thus the carbonyl complex **1**·BF_4 can be regarded as a precursor for **A** with *cis*-divacant sites (Scheme 1).

Dimethyl sulfide, SMe_2, bearing two lone pair electrons, also readily reacted with **1**·BF_4 to give a brown product **6**·BF_4 (Scheme 7). Replacement of CO ligands is evident from (i) the single CO vibration, (ii) appearance of NMR signals for SMe_2, and (iii) the ESI-MS peak for the cationic part [m/z = 788: $(SMe_2)Rh_2$(PNNP)$(CO)_2$]. Taking into account the result of the reaction with isonitrile and the stoichiometry [1 (SMe_2):1 (Rh_2(PNNP))], the two inner CO ligands in **1**·BF_4 should be replaced by the two lone pair electrons of SMe_2. It is

(16) See, for example: Jiang, F.; Yap, G. P. A.; Pomeroy, R. K. *Organometallics* **2002,** *21,* 773. See also references therein.

(17) Brookhart, M. S. *Prog. Inorg. Chem.* **1988**, *36*, 1.

(18) Yamamoto, A. *Organotransition Metal Chemistry*; Wiley-Interscience: New York, 1986. Collman, J. P.; Hegedus, L. S.; Norton, J. R.; Finke, R. G. *Principles and Applications of Organotransition Metal Chemistry*, 2nd ed.; University Science Books: Mill Valley, CA, 1987. Crabtree, R. H. *The Organometallic Chemistry of the Transition Metals*, 3rd ed.; Wiley-Interscience: New York, 2001.

Scheme 8

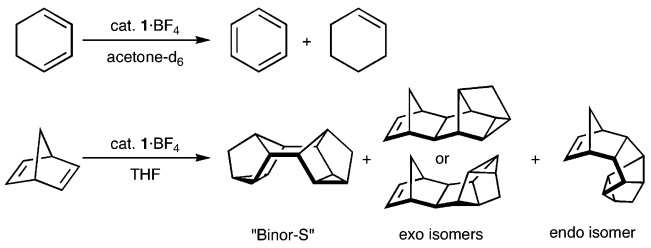

also revealed that the coordinated SMe_2 ligand exchanges with an external SMe_2 molecule at room temperature, because (i) a single Me_2S resonance (^{1}H NMR) is observed even in the presence of excess SMe_2 and (ii) addition of an excess amount of SMe_2 causes a shift of the SMe_2 signal to the signal for free SMe_2.

3-Hexyne, an internal acetylene, did not react with **1**·BF_4 at ambient temperature, but refluxing in acetone led to formation of the brown product **7**·BF_4 (Scheme 7), which was so labile that attempted purification by crystallization caused elimination of the 3-hexyne ligand to give an intractable mixture of products. Spectroscopic data of **7**·BF_4 consistent with apparent C_{2v}-symmetrical structural features (a single set of NMR resonances for the CH_2P and C−CH_2CH_3 moieties) suggest symmetrical μ-η^2:η^2-coordination of 3-hexyne, and the coordinated alkyne carbon signal is located at δ_C 76.9, which is comparable to that in (μ-η^2:η^2-H−C≡C−H)$Co_2(CO)_6$ (δ_C 70.8).[19] Reaction of **1**·BF_4 with R−C≡C−R (R= Ph, COOMe) was slow and sluggish, and after a prolonged reaction period complicated mixtures were obtained. On the other hand, 1-alkynes afforded tetranuclear product **8**·BF_4 resulting from ≡C−H cleavage as described below.

Complex **1**·BF_4 was inert toward alkenes such as 1-hexene and cyclopentene, whereas catalytic transformations were observed for dienes (Scheme 8). 1,3-Cyclohexadiene underwent disproportionation at ambient temperature to give an equimolar mixture of benzene and cyclohexene in the presence of a catalytic amount of **1**·BF_4. Dimerization of norbornadiene (NBD) was also catalyzed by the action of **1**·BF_4. The reaction in THF at room temperature caused quantitative conversion of 13 equiv of NBD into "Binor-S" (a 4+4 adduct) within 4 days. When the reaction was carried out in refluxing THF, more than 150 equiv of NBD was consumed within 10 h, but a mixture of isomeric products containing *exo*- (46%) and *endo*-isomers (8%) of the 4+2 adduct in addition to Binor-S (48%) was obtained. Because no characterizable rhodium species could be detected, the reaction mechanism remains to be studied. Many complexes were reported to catalyze the dimerization of NBD,[20] but we found that Rh−diene complexes such as [Rh(η^4-NBD)$_2$]$^+$ and [(η^4-NBD)$_2$$Rh_2$-(PNNP)]$^+$ (precursors for **1**·BF_4) were not effective.

Scheme 9

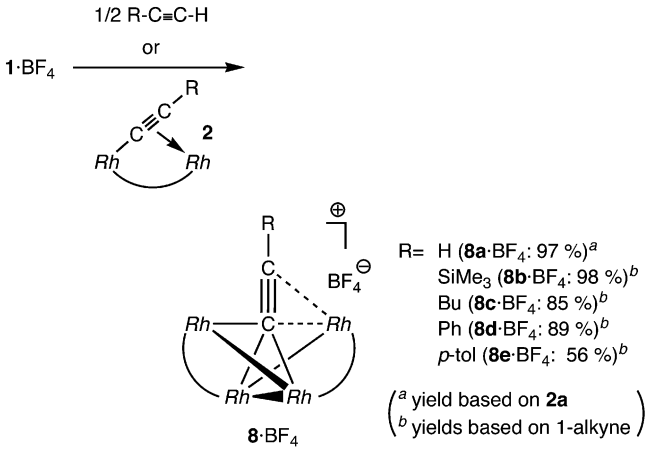

Reactions with butadiene, isoprene, and cyclopentadiene gave mixtures of unidentified organometallic species, whereas unconjugated diene such as 1,5-cyclooctadiene left **1**·BF_4 unaffected.

II. Tetranuclear Complexes. Unexpected formation of unique tetranuclear adducts [(μ_4-X)Rh_4(PNNP)$_2$]$^{n+}$, which resulted from a 1 (X):2 [Rh_2(PNNP)] coupling, was noted for interaction of **1**·BF_4 with 1-alkyne, hydrosilane, and water, and their structures were dependent on X.

Interaction of 1·BF_4 with 1-Alkyne Leading to Tetranuclear μ_4-Acetylide Complexes [(μ_4-C≡C−R)Rh_4(PNNP)$_2$(CO)$_4$]BF_4, 8·BF_4. In contrast to the above-mentioned reactions of **1**·BF_4 with substrates containing a C≡C functional group, which afforded dinuclear products, i.e., μ-acetylide complex **2** (with lithium acetylides) and μ-η^2:η^2-alkyne complex **7**·BF_4 (with 3-hexyne), interaction with 1-alkynes led to the formation of the tetranuclear μ_4-acetylide cluster complexes **8**·BF_4.

(i) Synthesis and Characterization of 8·BF_4. Reaction of **1**·BF_4 with 1-alkyne (R = $SiMe_3$, n-Bu, Ph, *p*-tol) in acetone afforded deep purple-red tetranuclear μ_4-acetylide complexes **8b**−**e**·BF_4 as sole products in good yields (Scheme 9).[21] Even in the presence of an excess amount of 1-alkyne, **8b**−**e**·BF_4 were formed as single products. The tetranucelar complexes **8a**−**e**·BF_4 were also obtained by addition of the Rh_2 fragment (**1**·BF_4) to the dinuclear μ-acetylide complex **2**.

^{1}H NMR and the ESI-MS spectra of **8**·BF_4 reveal formation of cationic tetranuclear acetylide complexes with the composition [(R−C≡C)Rh_4(PNNP)$_2$(CO)$_4$]$^+$ through a 1 (R−C≡C):2 [Rh_2(PNNP)] coupling, but complicated dynamic behavior is observed for them. For example, the *p*-tolylethynyl complex **8e**·BF_4 shows a single ^{31}P NMR resonance (δ_P 56.3) at 25 °C, which separates into two signals below −42 °C (Figure 4a).

(19) Aime, S.; Milone, L.; Rossetti, R.; Stanghellini, P. L. *Inorg. Chim. Acta* **1977**, *22*, 135.

(20) (a) Mitsudo, T.; Suzuki, T.; Zhang, S.-W.; Imai, D.; Fujita, K, Manabe, T.; Shiotsuki, M.; Watanabe, Y.; Wada, K.; Kondo, T. *J. Am. Chem. Soc.* **1999**, *121*, 1839. (b) Binger, P.; Albus, S. *J. Organomet. Chem.* **1995**, *493*, C6. (c) Gol'dshleger, N. F.; Azbel, B. I.; Isakov, Y. I.; Shipiro, E. S.; Minachev, K. M. *J. Mol. Catal. A: Chem.* **1996**, *106*, 159. (d) Acton, N.; Ronald, J. R.; Katz, T. J.; Frank, J. K.; Maier, C. A.; Paul, I. C. *J. Am. Chem. Soc.* **1972**, *94*, 5446. (e) Azbel, B. I.; Gol'dshleger, N. F.; Khidekel, M. L. *J. Mol. Catal.* **1987**, *40*, 57. (f) Kanai, H.; Watanabe, Y.; Nakayama, T. *Bull. Chem. Soc. Jpn.* **1986**, *59*, 1277. (g) Schrauzer, G. N.; Bastian, B. N.; Fosselius, G. A. *J. Am. Chem. Soc.* **1966**, *88*, 4890. (h) Schrauzer, G. N.; Ho, R. K. Y.; Schlesinger, G. *Tetrahedron Lett.* **1970**, *8*, 543.

(21) We also attempted synthesis of the Ir_4 and Rh_2Ir_2 derivatives. Although a dinuclear acetylide complex, (μ-η^1:η^2-C≡C−$SiMe_3$)Ir_2-(PNNP)(CO)$_2$, was obtained successfully, subsequent treatment with **1**·BF_4 gave a mixture of hetero- and homometallic tetranuclear complexes with the metal compositions of Ir_4, Ir_2Rh_2, and Rh_4 as observed by ESI-MS and ^{31}P NMR but could not be separated owing to their lability. This result also supports the dissociation equilibrium of **8**·BF_4 and its iridium analogue. On the other hand, reaction of [Ir_2-(PNNP)(CO)$_4$]BF_4 with hydrosilane resulted in Si−H oxidative addition. Dubs, C.; Inagaki, A.; Akita, M. Unpublished results.

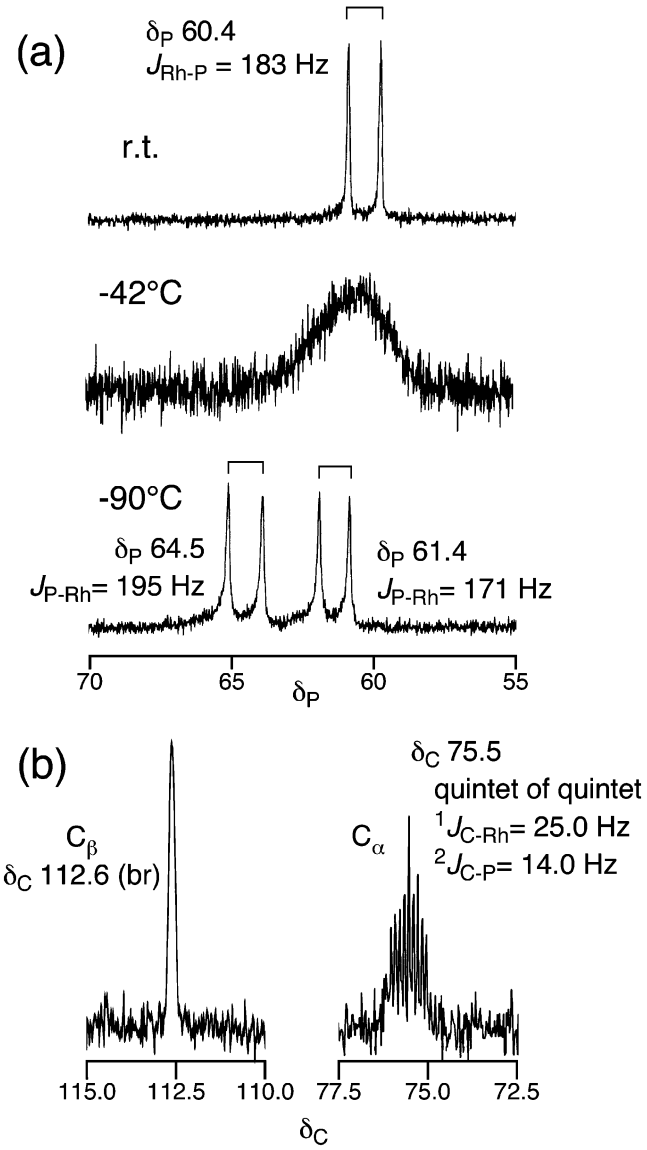

Figure 4. NMR spectra for **8a**·BF_4 observed in CD_2Cl_2: (a) variable-temperature ^{31}P NMR spectra observed at 81 MHz; (b) ^{13}C NMR spectra for the C≡C part observed at 25 °C at 100 MHz.

The two signals with different P−Rh coupling constants [**8a**$^+$: 195 Hz (δ_P 64.5); 171 Hz (δ_P 61.4)] reveal that **8a**$^+$ contains two types of rhodium atoms located in different environments. No further change is observed even when the sample is cooled to −90 °C. The fact that the J_{P-Rh} value at 25 °C (183 Hz) is precisely the average of the J_{P-Rh} values observed at −90 °C [(195 + 171)/2 = 183] confirms that the single δ_P signal at 25 °C results from coalescence of the two signals observed at low temperatures. In accord with the changes in the ^{31}P NMR spectrum, the acetylide $\delta_C(C_\alpha)$ signal, which appears at 25 °C as a quintet-of-quintets due to coupling with four equivalent RhP units (Figure 4b), changes into an irresolvable multiplet at low temperatures. The $\delta_C(C_\beta)$ signal appears as a broad one irrespective of temperatures presumably due to weaker interaction with the $[Rh_2(PNNP)]_2$ moiety compared with that of the C_α atom. The lack of $^1J_{C-H}$ coupling for the $\delta_C(C_\alpha)$ signal clearly indicates formation of an acetylide cluster compound resulting from cleavage of the ≡C−H bond in 1-alkyne, and the large J_{C-H} value for the C_β signal

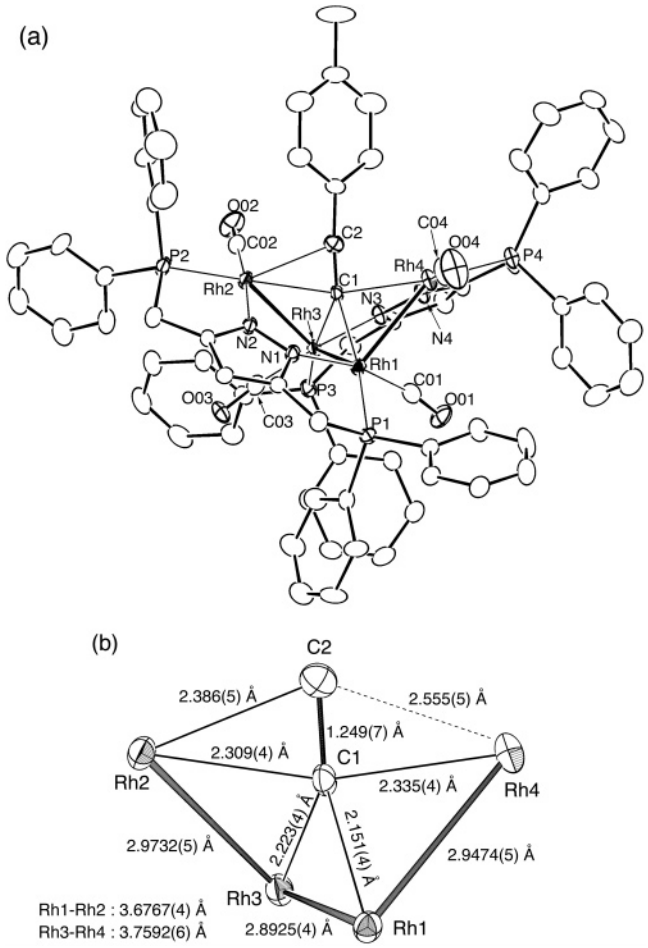

Figure 5. Molecular structures of the cationic part of **8e**·BPh_4 drawn with thermal ellipsoids at the 30% probability level: (a) an overview and (b) the core part.

for **8a**·BF_4 (237 Hz) reveals its sp-hybridization. Similar spectroscopic features are noted for the other products. These spectroscopic features suggest that (i) the Rh_4 metal framework is unsymmetrical with respect to the R−C≡C moiety, but exhibits dynamic behavior, which averages all Rh coordination environments at higher temperatures, and (ii) the acetylide part is coordinated to the Rh_4 framework in a μ_4-$\eta^1(C_\alpha)$:$\eta^2(C_\alpha{\equiv}C_\beta)$-fashion.

The *p*-tolylethynyl complex **8e**$^+$ was characterized by X-ray crystallography after conversion to the BPh_4 salt. ORTEP drawings for an overview and the core part of the cationic part are shown in Figure 5, and its selected structural parameters are listed in Table 4. Although the four rhodium atoms are arranged in a butterfly-like array,[1] it should be noted that the two Rh···Rh distances [Rh1···Rh2: 3.6767(4) Å; Rh3···Rh4: 3.7592(6) Å] exceed the range of bonding interaction, in contrast to the other Rh−Rh distances of ca. 2.9 Å (Table 4). The metal array observed for **8a**$^+$ is best described as a folded Z-shaped linkage. As is suggested by the spectroscopic data, the C_α atom of the acetylide ligand forms σ-bonding interactions with all four Rh centers and the C≡C moiety is π-bonded to one of the wingtip metal atoms (Rh2), leading to the μ_4-$\eta^1(C_\alpha)$:$\eta^2(C_\alpha{\equiv}C_\beta)$-coordination.[22]

Taking into account the structural features of **8**·BF_4, a canonical resonance structure **8′**·BF_4, which is apparently formed from **2** and **A**, can be depicted as shown in Scheme 10. Interaction of the Rh_C-C_α bonding

Table 4. Selected Structural Parameters for $[(\mu_4\text{-X})Rh_4(PNNP)_2(CO)_4]^{n+}$ [a]

complex	**8e**·BF_4	**9**	**10**	**11**
X	C≡C-*p*-tol	C_2	H	O
Rh1−X (X)	2.151(4) (C1), 3.257(5) (C2)	2.04(1) (C1)	1.70(5) (H1)	2.101(8) (O0)
Rh2−X (X)	2.309(4) (C1), 2.386(5) (C2)	2.438(8) (C1), 2.408(7) (C2)	2.05(5) (H1)	2.069(8) (O0)
Rh3−X (X)	2.223(4) (C1), 3.194(5) (C2)	2.06(1) (C2)	1.99(4) (H1)	2.089(9) (O0)
Rh4−X (X)	2.335(4) (C1), 2.555(5) (C2)	2.396(7) (C1), 2.441(8) (C2)	1.91(5) (H1)	2.085(8) (O0)
Rh1−P1, Rh2−P2	2.264(1), 2.235(1)	2.259(3), 2.230(2)	2.259(2), 2.238(2)	2.210(3), 2.209(3)
Rh3−P3, Rh4−P4	2.237(1), 2.218(1)	2.258(3), 2.219(2)	2.238(2), 2.256(2)	2.204(4), 2.210(3)
Rh1−N1, Rh2−N2	2.062(4), 2.042(4)	2.027(6), 2.079(7)	2.030(6), 2.037(6)	2.014(9), 2.059(7)
Rh3−N3, Rh4−N4	2.059(4), 2.052(4)	2.042(7), 2.069(8)	2.021(6), 2.020(6)	2.024(8), 2.046(9)
Rh1−C01, C01−O01	1.846(5), 1.152(6)	1.815(9), 1.15(1)	1.832(9), 1.14(1)	1.82(1), 1.15(2)
Rh2−C02, C02−O02	1.844(5), 1.138(7)	1.83(1), 1.14(1)	1.838(8), 1.15(1)	1.84(1), 1.15(1)
Rh3−C03, C03−O03	1.847(5), 1.146(6)	1.81(1), 1.16(1)	1.827(8), 1.15(1)	1.83(1), 1.16(1)
Rh4−C04, C04−O04	1.854(7), 1.118(8)	1.81(1), 1.16(1)	1.856(9), 1.12(1)	1.82(1), 1.14(2)
Rh1···Rh2, Rh1···Rh3	3.6767(4), 2.8925(4)	3.815(2), 5.162(1)	3.4730(8), 2.9083(9)	3.644(1), 3.113(1)
Rh1···Rh4, Rh2···Rh3	2.9474(5), 2.9732(5)	3.7615(8), 3.7826(8)	2.8890(7), 3.1022(6)	3.234(1), 3.149(2)
Rh2···Rh4, Rh3···Rh4	4.5943(6), 3.7592(6)	3.173(2), 3.849(1)	2.8969(8), 3.4153(6)	3.542(1), 3.651(2)
θ_2			86.9	91.5
α_1, α_2	15.4(2), 16.3(2)	18.9(4), 39.2(4)	14.6(2), 20.6(3)	4.5(4), 8.0(4)
α_3, α_4	25.4(2), 7.8(2)	−14.1(4), 28.1(5)	14.9(2), 12.9(2)	1.4(4), 7.7(4)
β_1, β_2		1.7, 11.0	14.6, 20.6	6.2, 4.5
β_3, β_4		4.5, 3.1	14.9, 12.9	5.0, 7.3
γ_{12}, γ_{34}	11.8(5), −7.1(6)	0(1), 15(2)	2.8(7), 3.5(7)	4(1), 8.3(9)

[a] Interatomic distances in Å and bond angles in deg. For α−γ (in deg), see Scheme 3. θ_2 (in deg): dihedral angles made by the Rh1−X−Rh2 and Rh3−X−Rh4 planes.

Scheme 10

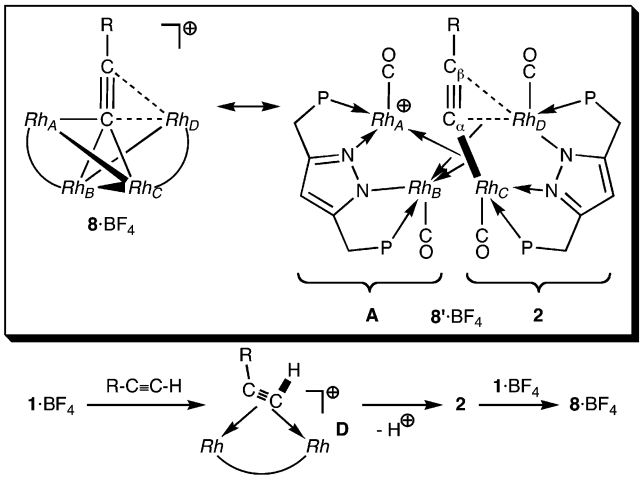

Scheme 11

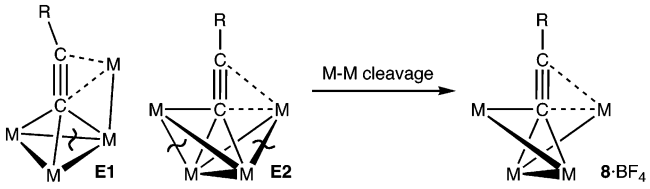

electrons with the Rh_A and Rh_B atoms and that of the Rh_D-C_α bonding electrons with the Rh_B atom lead to the tetranuclear structure **8′**·BF_4, and the interactions should originate from the highly electrophilic nature of **A**. The bonding scheme of **8′**·BF_4 suggests a formation mechanism of **8**·BF_4 from **1**·BF_4 and 1-alkyne as shown in Scheme 10. At the first stage of the reaction, 1-alkyne should be incorporated into the dirhodium system as a μ-η^2:η^2-coordinated ligand (**D**), as observed for **7**·BF_4. Deprotonation of the acidic ≡C−H proton in the cationic intermediate **D** should form the dinuclear μ-acetylide complexes **2**, which further interact with **1**·BF_4 to produce **8**·BF_4. In accord with this mechanism, (i) the reaction proceeds cleanly in a basic solvent such as acetone when compared with the reaction in a nonbasic solvent such as CH_2Cl_2 and (ii) treatment of an isolated sample of **2** with **1**·BF_4 produces **8**·BF_4, as described above (Scheme 9). The limiting structure **8′**·BF_4 indicates that (i) all metal centers are Rh(I) and (ii) the Rh_A, Rh_C, and Rh_D parts and the Rh_B part are regarded as four-coordinate structures with 16 valence electrons (VEs) and a five-coordinate structure with 18 VEs, respectively. Because the number of VEs in **8**·BF_4 (60 VEs) is equal to that of a Z-shaped tetranuclear metal array with three M−M bonds consisting of three 16 VE and one 18 VE fragments, the μ_4-acetylide complex **8**·BF_4 is concluded to be electron-precise.

The Z-shaped tetranuclear metal linkage is rather rare, and to the best of our knowledge, **8**·BF_4 is the first example of a $(\mu_4\text{-X})M_4$-type species with such a metal linkage. The Rh1−Rh3 connection causes a severe distortion of the structure, as is evident from the large α and γ values, and the conformation of the PNNP ligand in **8**·BF_4 is type I, as judged by the α values (Table 4). The interaction mode of the acetylide ligand in **8**·BF_4 is similar to μ_4-$\eta^1(C_\alpha)$:$\eta^2(C_\alpha{\equiv}C_\beta)$-acetylide cluster compounds with a spiked triangular (**E1**) and butterfly metal array (**E2**: Scheme 11).[21] Cleavage of one or two M−M bond(s) apparently leads to the framework observed for **8**·BF_4.

The temperature-dependent NMR behavior of $\mathbf{8}^+$ described above can be interpreted in terms of a combination of flipping of the acetylide ligand (process *a*), reorganization of the folded Z-shaped metal linkage (process *b*), and switching of the interactions of $Rh-C_\alpha$ bonding electrons (process *c*) (Scheme 12), although a spectrum at the slow exchange limit, which is consistent with the X-ray structure of $\mathbf{8e}^+$ with no element of symmetry, is not obtained. The former two processes can be regarded as modified versions of the well-

(22) Related μ_4-$\eta^1(C_\alpha)$:$\eta^2(C_\alpha{\equiv}C_\beta)$-acetylide cluster complexes with a butterfly or spiked triangular metal array are known. Sappa, E.; Tiripicchio, A.; Braunstein, P. *Chem. Rev.* **1983**, *83*, 203. Raithby, P. R.; Rosales, M. J. *Adv. Inorg. Chem. Radiochem.* **1985**, *29*, 169. Sappa, E.; Tiripicchio, A.; Carty, A. J.; Toogood, G. E. *Prog. Inorg. Chem.* **1987**, *35*, 437.

Scheme 12

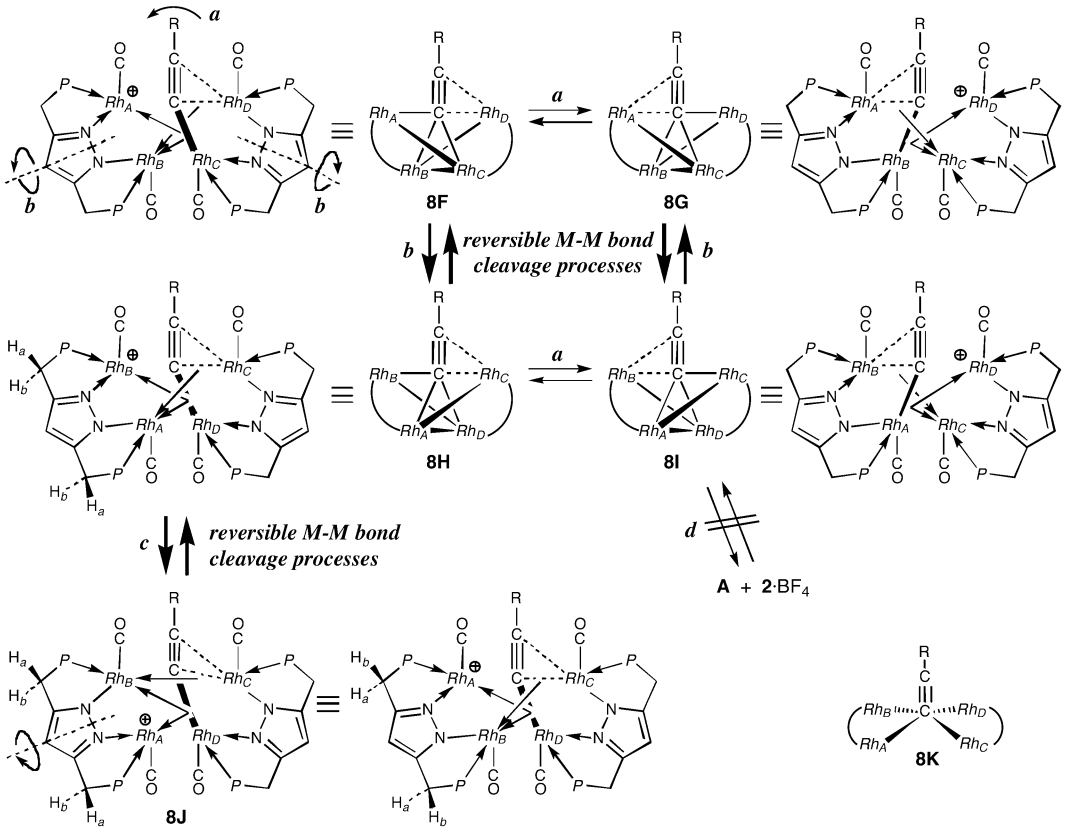

documented windshield wiper motion of the acetylide ligand:[7] between the wingtip metal atoms (process *a*) and between the intra-PNNP-ligand wingtip-hinge metal atoms (process *b*). Canonical structures are also shown in Scheme 12. In the interconversion *a* (**8F** ↔ **8G** and **8H** ↔ **8I**), switching of the η^2-coordination to the wingtip Rh centers (Rh_A and Rh_D) is associated with reorganization of the η^1- and η^2-interactions as well as switching of the Rh−C *σ*-bonding interaction (C_α-Rh_C → C_α-Rh_B). On the other hand, process *b* (**8F** ↔ **8H** and **8G** ↔ **8I**) involves switching of the η^1- and η^2-interactions in the part corresponding to **2** (Scheme 10), as observed for **2** (Scheme 4). It is notable that, in process *a*, the relative arrangement of the four metals is retained, whereas process *b* involves not only simultaneous rotation of the two PNNP ligands but also Rh−Rh bond cleavage and recombination processes to exchange the wingtip and hinge Rh centers. Furthermore process *a* + *b* cannot account for the CH_2P proton signals appearing as a single resonance at higher temperatures, because H_a atoms (proximal to the acetylide ligand) and H_b atoms (distal from the acetylide ligand) are left distinguishable. The H_a−H_b site exchange can be explained in terms of, for example, switching of interaction modes of the Rh_C−C_α *σ*-bonding electrons with Rh centers (from Rh_A (**8K**) to Rh_B (**8J**): process *c*), and accompanied rotation of the PNNP ligand renders H_a and H_b equivalent. An intermolecular mechanism via dissociation into **A** + **2** (process *d*) can be excluded on the basis of the following reasons. Although a related process was observed as described below (Scheme 13), its rate (∼30 min) was much slower than the time scale of coalescence of NMR signals and the negative activation entropy value ($\Delta S^{\ddagger} = -20.8$ eu, $\Delta H^{\ddagger} = 5.3$ kcal/mol) estimated

Scheme 13

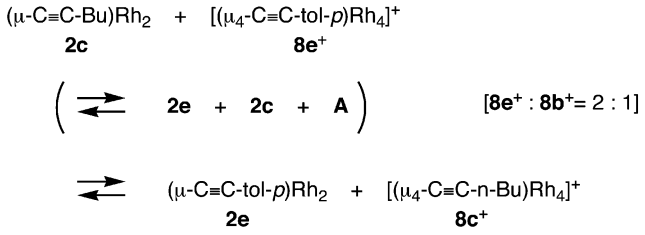

from the VT measurement of $\mathbf{8e}^+$ also supports an intramolecular mechanism. A C_{2v}-symmetrical intermediate **8K** cannot account for the H_a−H_b averaging process but cannot be excluded, because a combination with other rotation processes such as process *c* makes it possible to account for the dynamic behavior of **8**·BF_4.

The subtle difference in the C2−Rh2 and C2−Rh4 distances (∼0.17 Å) in **8e**·BPh_4 suggests that the lower energy process, which cannot be frozen out even at −90 °C, should be ascribed to the least motion process (process *a*). It is notable that the higher energy process *b* and the rotation process *c* involve reversible cleavage and recombination of the metal−metal bonds.

(ii) Exchange between Di- (2) and Tetranuclear Acetylide Complexes (8·BF_4).[22] To check the viability of a dissociation process for the dynamic behavior of the tetranuclear acetylide complex **8**·BF_4 (process *d* in Scheme 12), interaction between the dinuclear acetylide complex (**2**) and a tetranuclear complex containing a different acetylide substituent (**8**·BF_4) was followed by ^{1}H NMR (Scheme 13). As a result, a 1:1 mixture of **2c** and **8e**·BF_4 reached an equilibrium with the composition of $\mathbf{8e}^+$:$\mathbf{8c}^+$ = ∼2:1 during the course of 30 min. This result clearly indicates participation of a slow dissocia-

Scheme 14

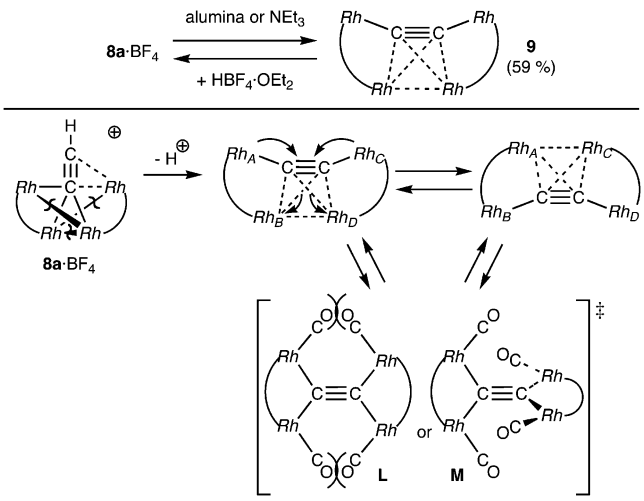

tion process, but the rate is much slower than the time scale of coalescence of NMR signals.

(iii) Deprotonation of 8a·BF_4 Leading to a μ_4-Dicarbide Cluster Compound, 9.[23] The NMR data for the ≡C−H part of the ethynyl complex **8a**·BF_4 (δ_H 6.82; J_{C-H} = 237 Hz) suggest its sp-hybridized, acidic character.[24] Actually, **8a**·BF_4 was acidic enough to be readily deprotonated upon treatment with alumina or NEt_3 to give the neutral C_2 (dicarbide) complex **9**,[25] and the deprotonation process could be reversed by addition of HBF_4·OEt_2 to **9** (Scheme 14).

The simple NMR features for **9** (single δ_C(C≡C) and δ_P signals), which do not change even when the sample is cooled as low as −90 °C, suggest formation of a symmetrical structure, and the ^{13}C NMR signal for the C_2 bridge is located at δ_C 98.9 (multiplet). X-ray crystallography of **9** (Figure 6 and Table 4) reveals the tetranuclear μ_4-dicarbide structure,[25] in which the C_2 bridge is interacted with each Rh_2(PNNP) fragment in a μ-η^1:η^2-fashion. The C≡C length [1.22(1) Å] is comparable to those in **2** and **8e**·BF_4, and the structure of the dinuclear moiety (μ-C_2)Rh_2(PNNP) is found to be similar to that of the dinuclear μ-acetylide complexes **2**. Complex **9** is a rare example of a (μ_4-η^1:η^1:η^2:η^2-C_2)-M_4-type dicarbide complex,[26] but, when compared with the previous examples, the (μ_4-C_2)M_4 moiety is folded to a considerable extent presumably (i) to avoid steric repulsion among CO ligands and (ii) to overlap with the two orthogonal π-orbitals of the central C_2 ligand in an effective manner. The dihedral angle between the C1−C2−Rh2 plane and the C1−C2−Rh4 plane is 94.8°, which is substantially more acute than the corresponding dihedral angle in [(μ_4-C_2)Cu_4(Ph_2Ppzpy)$_2$]$^{2+}$ (129.0°).[26b] In addition, because the Rh2−Rh4 separation [3.1723(7) Å] falls in the longer end of Rh−Rh bonds, the folding should result from an attractive interaction between the Rh2 and Rh4 atoms. The two Rh_2(PNNP) backbones adopt different conformations (type I for Rh1−Rh2 and type II for Rh3−Rh4). The inconsistency between the virtually C_2-symmetrical solid state structure with two different P-environments and the single ^{31}P NMR signal is due to dynamic behavior via oscillation of the C_2 ligand, i.e., concurrent switching of the η^1- and η^2-coordination (Scheme 14),[26c] where the σ-bonded metal centers in one structure ($Rh_{A,C}$) move to the π-bonded sites in the other structure. Of two viable transition states, the planar (**L**) and twisted one (**M**), the latter should be plausible, because (i) in the case of the related complexes **2**, steric hindrance between the CO ligand and the acetylide substituent (R) causes distortion of the structure (see above) and the twisted conformation **M** can minimize such interactions and (ii) the two Rh_2(PNNP)$(CO)_2$ fragments can effectively overlap with the two orthogonal π-orbitals of the C≡C moiety. The activation barrier for the fluxional process is very low, because the process cannot be frozen out even at −90 °C. Notable is that (i) the fluxional behavior of **9** involves a cleavage process of the Rh−Rh interactions and (ii) the deprotonation−protonation sequence is associated with reversible M−M bond cleavage and recombination processes (Scheme 14).

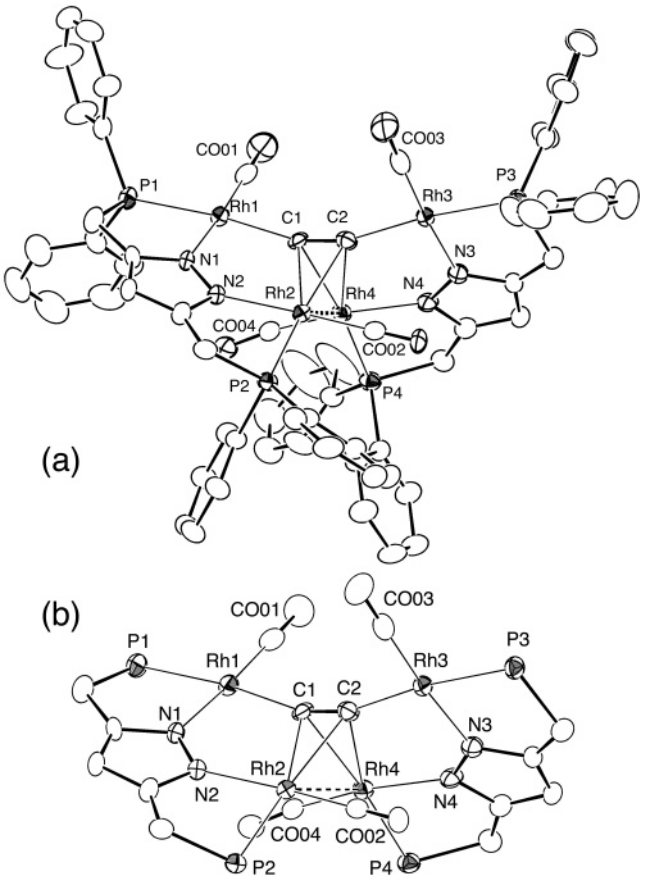

Figure 6. Molecular structures of the cationic part of **9** drawn with thermal ellipsoids at the 30% probability level: (a) an overview and (b) the core part.

Tetranuclear μ_4-Hydrido (10^+) and μ_4-Oxo Complexes (11). (i) Synthesis and Characterization. In

(23) The *p*-tolyl complex **8e**·BF_4 was subjected to reaction with nucleophiles. Reaction with Li−C≡C-*p*-tol and KOH gave **2e** and a mixture of **11** and **2e**, respectively, which were apparently formed via nucleophilic attack followed by dissociation into dinuclear fragments. The reaction with H_2SiPh_2 gave a mixture containing **10**·BF_4.

(24) Akita, M.; Terada, M.; Oyama, S.; Sugimoto, S.; Moro-oka, Y. *Organometallics* **1991**, *10*, 1561. Akita, M.; Takabuchi, A.; Terada, M.; Ishii, N.; Tanaka, M.; Moro-oka, Y. *Organometallics* **1994**, *13*, 2516. See also ref 9.

(25) Bruce, M. I.; Low, P. J. *Adv. Organomet. Chem.* **2004**, *50*, 180. See also: Akita, M.; Moro-oka, Y. *Bull. Chem. Soc. Jpn.* **1995**, *68*, 420, and references therein.

(26) (a) Bruce, M. I.; Snow, M. R.; Tiekink, E. R. T.; Williams, M. L. *Chem. Commun.* **1986**, 702. (b) Song, H.-B.; Wang, Q.-M.; Zhang, Z.-Z.; Mak, T. C. W. *Chem. Commun.* **2001**, 1658. (c) Lo, W.-Y.; Lam, C.-H.; Fung, W. K.-M.; Sun, H.-Z.; Yam, V. W.-W.; Balcells, D.; Maseras, F.; Eisenstein, O. *Chem. Commun.* **2003**, 1260.

Scheme 15

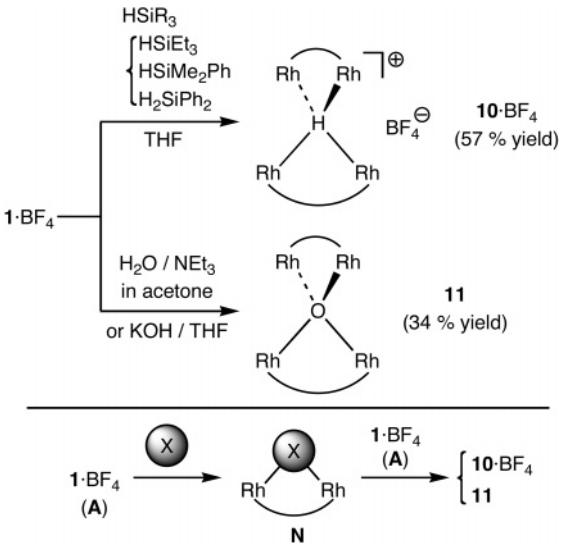

contrast to the acetylide cluster complexes $\mathbf{8}^+$ with the folded Z-shaped metal array described above, symmetrical and isostructural μ_4-hydride ($\mathbf{10}^+$) and μ_4-oxo complexes (**11**) with a tetrahedral metal array were produced from $\mathbf{1}\cdot BF_4$ (Scheme 15).

When a THF solution of $\mathbf{1}\cdot BF_4$ was treated with hydrosilanes such as $HSiEt_3$, $HSiMe_2Ph$, and H_2SiPh_2, the purple product $\mathbf{10}\cdot BF_4$ showing the complicated hydride ^1H NMR signal (Figure 7a) precipitated out of the mixture (Scheme 15).[22,27] On the other hand, reaction of $\mathbf{1}\cdot BF_4$ with NEt_3 in the presence of water or KOH

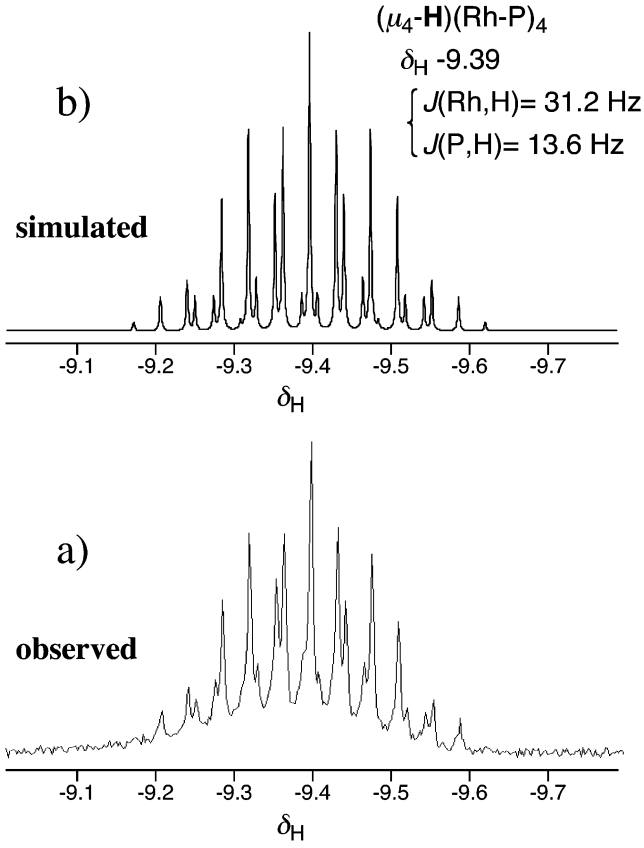

Figure 7. ^1H NMR spectra of $\mathbf{10}\cdot BF_4$ observed at 400 MHz (hydride region): (a) an observed spectrum (in CD_2Cl_2); (b) a simulated spectrum.

in THF gave a neutral orange product **11**, which was characterized as a μ_4-oxo complex (Scheme 15).

For the purple complex $\mathbf{10}\cdot BF_4$, the intensity of the hydride signal (^1H NMR) and an ESI-MS spectrum [*m/z* = 1451 (the molecular ion peak for $\mathbf{10}^+$)] suggest formation of a dimeric species formulated as $[(H)Rh_4(PNNP)_2(CO)_4]^+$. Because the same product is obtained irrespective of the hydrosilane used, the hydrosilane should serve as a hydride donor and the reaction of $\mathbf{1}\cdot BF_4$ with D_2SiPh_2 results in selective deuteration of the bridging hydride ($\mathbf{10}$-$d_1\cdot BF_4$), as confirmed by ^1H NMR and ESI-MS analyses. As for the spectral features of the $Rh_2(PNNP)(CO)_2$ moiety of $\mathbf{10}\cdot BF_4$, only a single set of signals for the CH_2PPh_2 (^1H, ^{13}C, and ^{31}P NMR), pyrazolyl (^1H and ^{13}C NMR), and CO moieties (IR and ^{13}C NMR) is observed, suggesting a 4-fold symmetrical structure. In addition, the complicated hydride signal has been successfully analyzed as a result of coupling with four equivalent Rh−P units ($^1J_{H-Rh}$ = 31.2 Hz, $^2J_{H-P}$ = 13.6 Hz; Figure 7b).[28] No apparent change of the ^1H (Rh−H) and ^{31}P NMR signals is detected upon cooling to −80 °C. These spectral data are consistent with a tetrarhodium complex with a tetrahedral or square-planar Rh_4 array connected by a symmetrically bridging μ_4-hydrido ligand, $[(\mu_4\text{-}H)[Rh_4(PNNP)_2(CO)_4]\text{-}BF_4$. The μ_4-oxo complex **11** shows NMR features very similar to those of the μ_4-H complex $\mathbf{10}^+$ except for lack of the hydride signal, indicating an analogous structure of 4-fold symmetry.

Crystallographic characterization was performed for $\mathbf{10}\cdot BPh_4$ (the BPh_4 salt of $\mathbf{10}^+$) and **11**. Overviews of their metallic parts are shown in Figure 8 together with expanded views of their core parts, and selected structural parameters are listed in Table 4. The hydride atom (H1) in $\mathbf{10}\cdot BPh_4$ was refined isotropically. The two $Rh_2(PNNP)(CO)_2$ subunits are arranged almost perpendicular to each other (see θ_2) to form Rh_4 tetrahedrons, and the bridging atoms (H1 and O0) are located in the middle of the Rh_4 tetrahedrons, as is consistent with the spectral data suggesting symmetrical structures. The Rh−X−Rh angles are in the range 93−134° with average values of 109.9° ($\mathbf{10}^+$) and 109.4° (**11**) [$\mathbf{10}^+$: Rh1−H1−Rh4: 105.9°, Rh4−H1−Rh3: 121.6°, Rh1−H1−Rh3: 103.3°, Rh4−H1−Rh2: 93.7°, Rh1−H1−Rh2: 135.0°, Rh3−H1−Rh2: 99.9°; **11**: Rh1−O0−Rh2: 121.8(3)°, Rh1−O0−Rh3: 96.0(4)°, Rh1−O0−Rh4: 101.2(4)°, Rh2−O0−Rh3: 98.4(4)°, Rh2−O0−Rh4: 117.0(4)°, Rh3−O0−Rh4: 122.0(3)°]. As for Rh···Rh separations in $\mathbf{10}\cdot BPh_4$, those between the two $Rh_2(PNNP)(CO)_2$ subunits are in the range 2.89−3.10 Å, which are substantially longer than the sum of the atomic radii of Rh (2.68 Å)[29] but shorter than the intraligand Rh···Rh separations (~3.4 Å), whereas, for **11**, the interunit Rh···Rh separations (3.11−3.54 Å) are comparable to the intraligand ones (~3.6 Å). A Rh−Rh bonding interaction, if present, should induce distortion of the square-planar coordination geometry of the d^8 metal center [Rh(I)]. Because, however, the four Rh

(27) Reaction of $\mathbf{1}\cdot BF_4$ with $LiHBEt_3$ or $NaBH_4$ did not afford $\mathbf{10}\cdot BF_4$ but a mixture of unidentified products.

(28) NMR simulation and EHMO calculations were performed with gNMR (ver. 3.6) and CAChe (ver. 4.0), respectively. The atomic coordinates for the EHMO calculation of $\mathbf{10H}^+$ were taken from the X-ray result, and the PH_2 hydrogen atoms were located at the calculated positions.

(29) Emsley, J. *Elements,* 2nd ed.; OUP: Oxford, 1998.

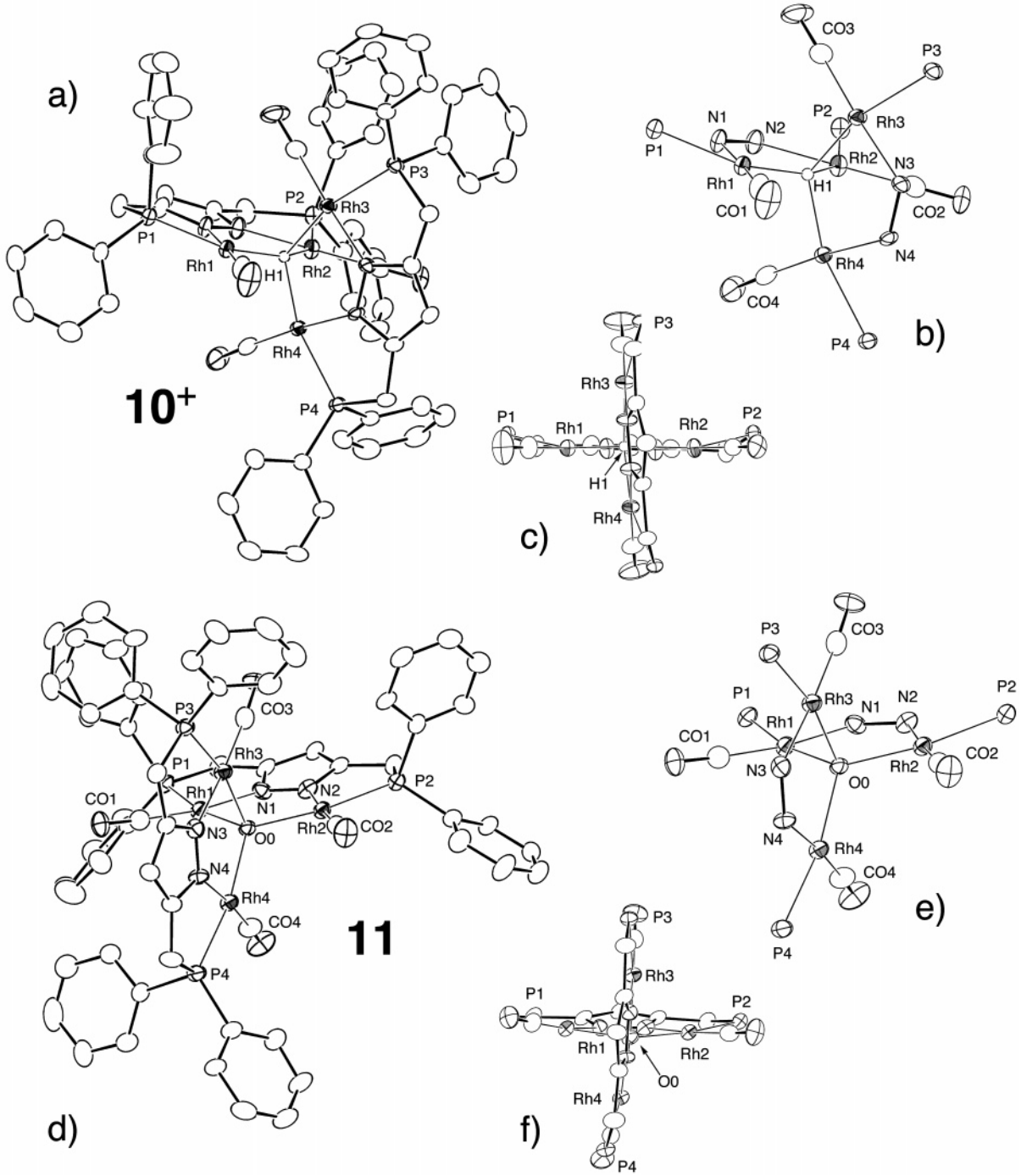

Figure 8. Molecular structure of the cationic part of **10**·BPh_4 and **11** drawn at the 30% probability level: (a, d) overviews; (b, e) expanded views of the core parts; (c, f) side views of the core parts.

coordination planes for **10**·BPh_4 and **11** are virtually planar, as judged by the β values, the Rh−Rh bonding interaction is negligible for them. When the core structures are inspected in detail, the Rh_4 tetrahedrons are distorted to a small extent. The side views and the positive α values show that, in both of the Rh_2(PNNP)-$(CO)_2$ subunits, the two five-membered $RhPC_2N$ chelates are slightly folded in the same direction to lead to type I conformations (Scheme 3), and the structure of **10**·BPh_4 is more distorted than that of **11**. The very small hydrogen atom connecting the four rhodium atoms in **10**·BPh_4 causes shrinking of the central five-membered XRh_2N_2 rings and the close Rh···Rh contacts as well. A detailed discussion on the Rh···Rh interactions will be presented in the next section.

Complexes **10**·BF_4 and **11** should be formed via a two-step mechanism through **N**(X = H/O) (Scheme 15) in a manner similar to that proposed for **8**·BF_4 (Scheme 10). In the presence of a base, a water molecule is finally converted to an oxo ligand (**11**) via double deprotonation.

Despite the isostructural feature, a significant difference is noted for electron counting. In contrast to the μ_4-oxo complex **11** with an electron-precise 64e configuration (16e × 4), the μ_4-hydrido complex **10**·BF_4 turns out to be a highly electron-deficient species with 58 valence electrons. Such an unsaturated electronic struc-

Scheme 16

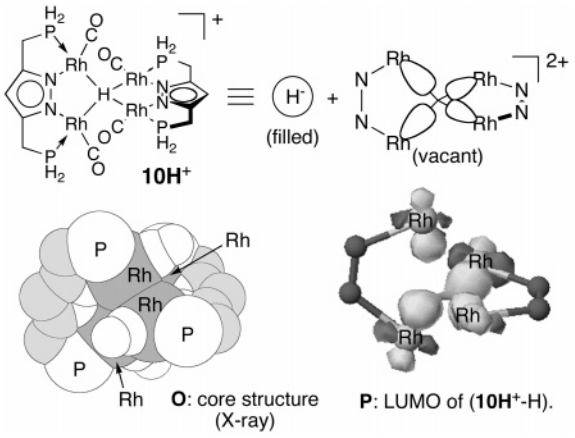

ture should be kinetically stabilized by the bulky PNNP ligands surrounding the Rh_4 tetrahedron, and the bridging hydrido ligand encapsulated in the Rh_4 tetrahedron is shielded from the outside (**O**: Scheme 16) so that **10**·BF_4 is stable even in CH_2Cl_2. Preliminary EHMO analysis[28] for a simplified H-substituted model (**10H**$^+$) reveals that the tetranuclear structure is formed by interaction of the filled hydride 1s orbital with the LUMO of the tetranuclear $[Rh_4(PNNP)_2(CO)_4]^{2+}$ fragment (**P**: Scheme 16), where the four σ-type Rh d orbitals of in-phase combination are projected toward the center of the Rh_4 tetrahedron, i.e., the position of the μ_4-hydrido ligand. A similar MO feature was noted for the μ_4-H tetratungsten cluster compound, $[(\mu_4\text{-H})W_4(OCH_2tBu)_{12}]^-$.[30a,b]

(ii) μ_4-Hydride Complex 10$^+$. A bridging hydride is a key structural feature of transition metal cluster compounds,[1] and a number of cluster compounds containing doubly (μ) and triply (μ_3) bridging hydrido ligands are known. Compounds with a hydrido ligand bridging more than three metal atoms, however, are still rare (Scheme 17). To the best of our knowledge, one μ_4- and one μ_5-hydride complex have been reported so far in addition to several examples of μ_6-hydride complexes with an octahedral M_6 array, and only three structural types **Q**−**S** are characterized for μ_n-H complexes ($n \geq 4$).[30,31] Furthermore the multiply bridging hydrido ligands in all the previous examples are associated with cluster

Scheme 17

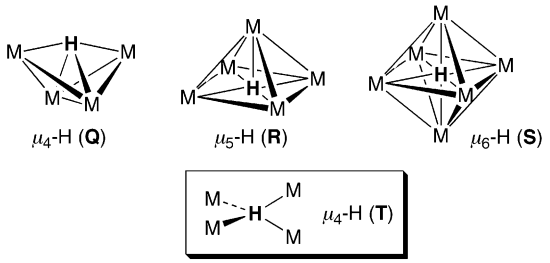

frameworks as in **Q**−**S**. Thus the μ_4-hydrido complex **10**·BPh_4 is characterized as the first example of a **T**-type μ_4-hydride in a discrete molecule (cation) and is found to be the second example of a structurally characterized $(\mu_4\text{-H})M_4$ complex following $[(\mu_4\text{-H})W_4(OCH_2tBu)_{12}]^-$,[30a,b] in which the μ_4-hydrido ligand is supported on a butterfly M_4 cluster framework (**Q**).

The present result reveals that support by a metal−metal bonded cluster framework is not essential for multiply bridging hydride (μ_n-H: $n \geq 4$). In all the previous examples (**Q**−**S**; Scheme 17) the multiply bridging hydrido ligand appears to be protected by the cluster framework, whereas in **10**$^+$, the hydride is not accommodated in a cavity formed by the metal framework but binds the four isolated rhodium centers (not connected by metal−metal bonds) together. The Rh−H binding force is strong enough to bring the Rh centers to the distances comparable to the sum of the atomic radii.

(iv) μ_4-Oxo Complex 11. The $(\mu_4\text{-O})M_4$ subunit with a tetrahedral metal array is one of key structural motifs of polyoxometalates and is also found for many first-row transition metal complexes, but examples of late transition metal complexes are rare.[32]

III. Features of Rh_2(PNNP) and Rh_4(PNNP)$_2$ Systems. Formation of Di- and Tetranuclear Complexes. The transformations of **1**·BF_4 reported in the present contribution are summarized in Scheme 18. The $Rh_2(PNNP)(CO)_2$ fragment **A** accommodates a variety of organic fragments, which are diverse with respect to not only their size but also their electronic structure. The dirhodium fragment **A** serves as an acceptor for substrates with up to four valence electrons (Scheme 18). 4e-Donors such as acetylide, vinyl, alkyne, $(CN-R)_2$, and SMe_2 and internal alkyne fit the electronic and structural demands of **A** to provide the dinuclear adducts **2**−**7** (**N**).

In the formation of the μ_4-acetylide complex **8**$^+$ and the μ_4-oxo complex **11**, a noncoordinated electron pair on the bridging ligand X in the coordinatively saturated

(30) μ_4-H: $[(\mu_4\text{-H})W_4(OCH_2tBu)_{12}]^-$: (a) Budzichowski, T. A.; Chisholm, M. H.; Huffman, J. C.; Eisenstein, O. *Angew. Chem., Int. Ed. Engl.* **1994**, *33*, 191. (b) Budzichowski, T. A.; Chisholm, M. H.; Huffman, J. C.; Kramer, K. S.; Eisenstein, O. *J. Chem. Soc., Dalton Trans.* **1998**, 2563. μ_5-H: $[(\mu_5\text{-H})_2Rh_{13}(CO)_{24}]^{3-}$: (c) Bau, R.; Drabnis, M. H.; Garlaschelli, L.; Klooster, W. T.; Xie, Z.; Koetzle, T. F.; Martinengo, S. *Science* **1997**, *275*, 1099, and references therein. μ_6-H: $[(\mu_6\text{-H})Ni_{12}(CO)_{21}]^{3-}$: (d) Broach, R. W.; Dahl, L. F.; Longoni, G.; Chini, P.; Schultz, A. J.; Williams, J. M. *Adv. Chem. Ser.* **1978**, *167*, 93. $[(\mu_6\text{-H})Ru_6(CO)_{18}]^-$: (e) Eady, C. R.; Johnson, B. F. G.; Lewis, J.; Malatesta, M. C.; Machin, P.; McPartlin, M. *J. Chem. Soc., Chem. Commun.* **1976**, 945. (f) Jackson, P. F.; Johnson, B. F. G.; Lewis, J.; Raithby, P. R.; McPartlin, M.; Nelson, W. J. H.; Rouse, K. D.; Allibon, J.; Mason, S. A. *J. Chem. Soc., Chem. Commun.* **1980**, 295. (g) Mul, W. P.; Elsevier: C. J.; Vuurman, M. A.; Smeets, W. J. J.; Spek, A. L.; de Boer, J. L. *J. Organomet. Chem.* **1997**, *532*, 89. $[(\mu_6\text{-H})Co_6(CO)_{15}]^-$: (h) Hart, D. W.; Teller, R. G.; Wei, C.-Y.; Bau, R.; Longoni, G.; Campanella, S.; Chini, P.; Koetzle, T. F. *Angew. Chem.* **1979**, *91*, 86; *Angew. Chem., Int. Ed. Engl.* **1979**, *18*, 80. (i) Hart, D. W.; Teller, R. G.; Wei, C.-Y.; Bau, R.; Longoni, G.; Campanella, S.; Chini, P.; Koetzle, T. F. *J. Am. Chem. Soc.* **1981**, *103*, 1458. $[(\mu_6\text{-H})Ru_7(CO)_{19}(\mu\text{-CNMe}_2)$: (j) Adams, R. D.; Babin, J. E.; Tanner, J. T. *Organometallics* **1988**, *7*, 2027. $[(\mu_6\text{-H})Cr_6]$: (k) Kamiguchi, S.; Imoto, H.; Saito, T.; Chihara, T. *Solid State Sci.* **1999**, *1*, 497. (l) Kamiguchi, S.; Saito, T.; Honda, Z. *J. Organomet. Chem.* **2000**, *609*, 184.

(31) Recently, a $(\mu_4$-hydrido)tetrapalladium complex with a puckered M−M bonded Pd_4-square skeleton, $[(\mu_4\text{-H})Pd_4(\mu\text{-dppm})_4]^+$, was reported, but the hydride ligand was not characterized by ^{1}H NMR and X-ray crystallography. Although an MO analysis suggested location of the hydride in the center of the Pd_4-square, the possibility of fluxional behavior of the hydride was not eliminated. Evrard, D.; Meilleur, D.; Drouin, M.; Mugnier, Y.; Harvey, P. D. *Z. Anorg. Allg. Chem.* **2002**, *628*, 2286.

(32) Ru: Gould, R. O.; Jones, C.L.; Stephenson, T. A.; Tocher, D. A. *J. Organomet. Chem.* **1984**, *264*, 365. Lavigne, G.; Lugan, N.; Kalck, P.; Soulie, J. M.; Lerouge, O.; Saillard, J. Y.; Halet, J. F. *J. Am. Chem. Soc.* **1992**, *114*, 10669. Maurette, L.; Donnadieu, B.; Lavigne, G. *Angew. Chem., Int. Ed.* **1999**, *38*, 3707. Pd: Zhang, Y.; Puddephatt, R. J.; Manojlovic-Muir, L.; Muir, K. W. *Chem. Commun.* **1996**, 2599. Os: Gould, R. O.; Jones, C. L.; Stephenson, T. A.; Tocher, D. A. *J. Organomet. Chem.* **1984**, *264*, 365. Au: Schmidbaur, H.; Hofreiter, S.; Paul, M. *Nature (London)* **1995**, *377*, 503.

Scheme 18

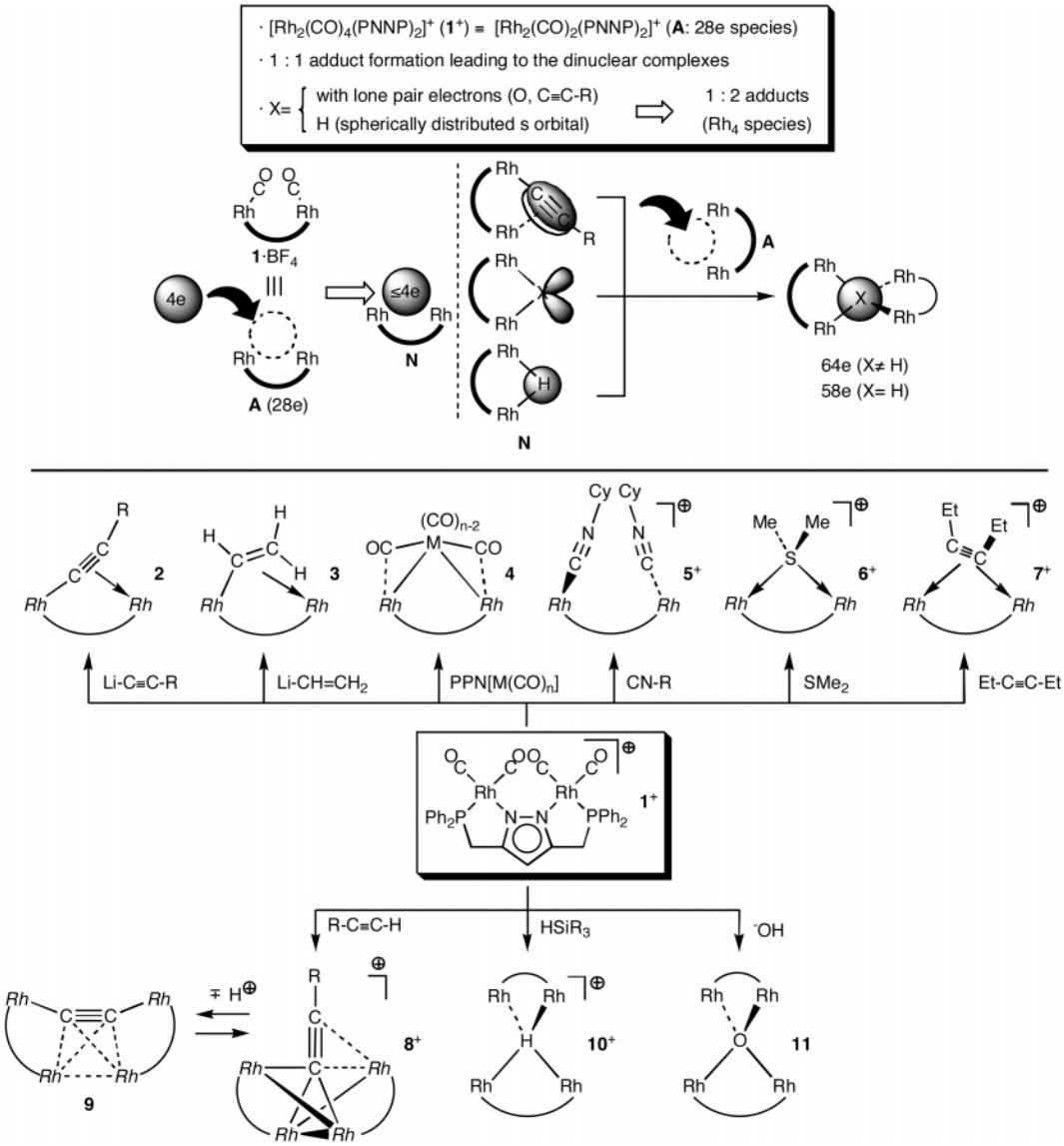

dinuclear intermediate **N** [π-electrons of the μ-acetylide ligand in **2** and the lone pair electrons of the bridging OH group in **N**(X = OH)] is used to interact with a second **A** fragment to lead to the dimeric tetranuclear structures with 64 VEs, $\mathbf{8}^+$ and **11**.

In contrast to these cases, the dinuclear intermediate **N**(X = H) for the μ_4-hydride complex $\mathbf{10}^+$ is an electron-deficient species with 30 VEs (cf. 32e for a saturated species), and despite such an electronic configuration, it further interacts with **A** to lead to the dimeric structure $\mathbf{10}^+$. In this case, **A** interacts with the 1s orbital of the bridging hydrogen atom in **N**(X = H), indicating that, even if (i) **N**(X = H) is an electron-deficient species and (ii) a noncoordinated electron pair as in **2** and **N**(X = OH) is not available for **N**(X = H), **A** is electrophilic enough to interact with the spherically distributed electrons of the filled 1s orbital of the bridging hydrogen atom in **N**(X = H) to give $\mathbf{10}^+$. The high electrophilicity of **A** is also supported by the reaction type. While a typical reaction expected for interaction of a coordinatively unsaturated organometallic species with hydrosilane is oxidative addition of its H−Si bond giving a hydrido-silyl species,[33] in the present system, simple hydride transfer leads to $\mathbf{10}\cdot BF_4$.

Because the dinuclear intermediate **N** cannot be detected during the formation of the tetranucelar complexes, the second step giving the 1:2 adduct should be faster than the initial step giving the 1:1 adduct **N**. The electron density at X in **N** should be larger than that in the starting compounds (X) to make the second step much faster, because interaction of X with the electropositive metal fragment may cause an increase of electron density, for example, via back-donation.

Flexibility of the $Rh_2(PNNP)(CO)_2$ Backbone.[34] As we expected, the Rh_2(PNNP) system (**A**) provides a *cis*-divacant coordination site, which can fit substrates (X) ranging from a small one such as a hydrogen atom ($\mathbf{10}\cdot BF_4$) to a bulky one such as $M(CO)_n$ (**4**). The Rh···Rh separations for the di- and tetranuclear complexes obtained by the present study are compared in Scheme 19, and they are divided into intraligand and interunit separations. The intraligand Rh···Rh separations, which exceed the Rh−Rh single bond length (<3.3

(33) Patai, S.; Rappoport, Z. *The Chemistry of Organosilicon Compounds*; Wiley: New York, 1989. See also ref 18 and references therein.

(34) Another apparent feature is the J_{P-Rh} values, which vary in a wide range [130 ($\mathbf{1}\cdot BF_4$)−200 Hz ($\mathbf{10}\cdot BF_4$)] as summarized in Scheme 19, but no apparent relationship with nuclearity, structure, properties, and size of the bridging ligand and charge is evident.

Scheme 19

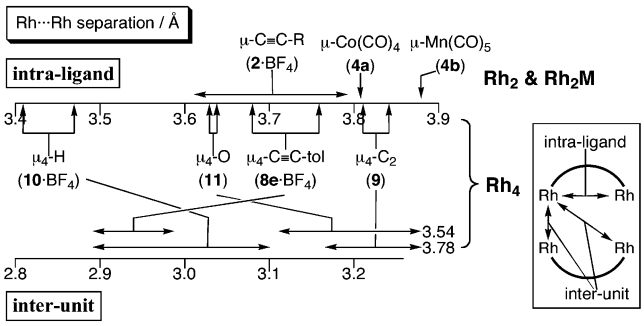

Scheme 20

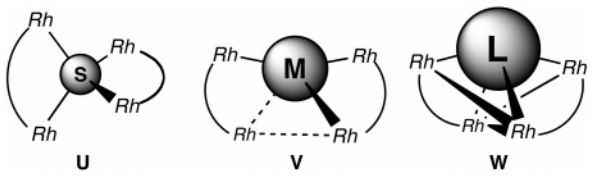

Å; see below), vary in the range 3.41−3.88 Å. Although the coordination modes are different, a roughly parallel relationship between the size of X and the intraligand Rh···Rh separation is evident.

Structures of the tetranuclear species depend on the size of the bridging ligand (X) (Scheme 20). When the size of X is small enough to be accommodated in the cavity in the $Rh_4(PNNP)_2$ part [e.g., H (**10**$^+$), O (**11**)], a symmetrical, tetrahedral structure (**U**) should be formed. In contrast, a bulky substrate such as an acetylide (**8e**$^+$) should deform the symmetrical structure (**W**), and a medium size species [e.g., C≡C (**9**)] should lead to an adduct **V** of an intermediate structural feature. The deformation from a symmetrical structure causes approach of the metal centers finally leading to a metal−metal bond, and therefore, the number of Rh−Rh interactions can be regarded as an index of the deformation. Accordingly, as going from **U** to **W**, the number of Rh−Rh interactions increases from 0 (**U**: **10**$^+$, **11**) to 1 (**V**: **9**) and then to 3 (**W**: **8e**$^+$).

Thus the Rh−PNNP system is flexible so as to fit a variety of substrates with different size and electronic properties.

Rh···Rh Interactions and Dynamic Behavior via Reversible M−M Bond Cleavage and Recombination Processes. The sum of the covalent radius of Rh is 2.68 Å,[29] but it is not always easy to determine the presence of a M−M bond solely on the basis of the M−M distance. According to the Cambridge Structural Database, the longest Rh−Rh bond is found for $[Rh_2(CN-C_6H_4-p-F)_8]^{2+}$ (3.293 Å)[35a] apart from the unusually long Rh−Rh separation for a dodecarhodium cluster compound (3.567 Å).[35b] Some of the interunit Rh···Rh interactions of the present tetranuclear complexes are shorter than 3.3 Å (Scheme 19).

A M···M bonding interaction is also evidenced by subsidiary structural parameters. For example, a M−M interaction of a square-planar metal fragment is frequently associated with (i) distortion to a five (or six) coordinate structure and/or (ii) semibridging CO ligands. In the case of the unsymmetrical structures of **8e**$^+$ and **9**, deviation from a square-planar coordination geometry is evident for Rh1−4 in **8e**$^+$ and Rh2,4 in **9**. In addition, in **8e**$^+$, the Rh1−C01−O01 [170.6(4)°] and Rh3−C03−O03 linkages [172.8(5)°] associated with the Rh1−Rh4 [2.9474(5) Å] and Rh2−Rh3 bonds [2.9432(5) Å] are considerably bent from a linear structure, and slight bending is apparent even for the Rh2−C02−O02 [176.6(5)°] and Rh4−C04−O04 linkages [175.6(7)°]. In the case of **9**, too, the Rh2−Rh4 bonding interaction [3.1727(9) Å] is associated with the Rh2−C02−O02 [173.4(7)°] and Rh4−C04−O04 semibridging ligands [172.4(7)°] [cf. Rh1−C01−O01: 179(1)°; Rh3−C03−O03: 179(1)°]. In contrast to these M−M bonded systems, the μ_4-hydrido (**10**$^+$) and μ_4-oxo complexes (**11**) contain four-coordinate square-planar Rh centers, as discussed above, and no systematic CO bending is found for them [Rh−C−O > 175°; **10**$^+$: Rh1−C1−O1: 177.7(8)°, Rh2−C2−O2: 179.5(6)°, Rh3−C3−O3: 178.5(8)°, Rh4−C4−O4: 177.9(7)°; **11**: Rh1−C1−O1: 176(1)°, Rh2−C2−O2: 177(1)°, Rh3−C3−O3: 175(1)°, Rh4−C4−O4: 177(1)°]. On the basis of these features, it is concluded that the (μ_4-X)Rh_4 species **10**$^+$ and **11** are not supported by metal−metal bonds.[36]

The structural discussion described above reveals that the polynuclear structures in the present system are integrated mainly through M−X interactions rather than M−M interactions. When some other steric constraints of the system (e.g., relief of steric repulsions) force two 16e metal centers to be brought close to each other, a M−M interaction should be formed.

One of the intriguing aspects of the present system is the dynamic property of the metal−metal bonds. The fluxional processes of the tetranuclear complexes **8**$^+$ and **9** involve reversible cleavage and recombination of Rh−Rh bonds (Scheme 12), and the Rh_4 species **8a**$^+$ and **9** are interconverted with each other via the protonation−deprotonation cycle associated with cleavage of the Rh−Rh interaction (Scheme 14). Such a behavior is still rare, and we previously reported related processes for trinuclear μ_3-acetylide cluster compounds containing a metal fragment as the acetylide substituent, $\{\mu_3\text{-}C{\equiv}C\text{-}FeCp^*(CO)_2\}FeM_2Cp^*(CO)_n$ (M/n = Co/8; Fe/7),[37] where the distal Fe center not included in the triangular FeM_2 frameworks exchanges with the Fe group in the FeM_2 triangle via reversible cleavage of the FeM_2 triangle and incorporation of the distal Fe group to form a new FeM_2 triangle. As discussed above, the Rh···Rh interactions in the present system are weak, and in consequence, the metal−metal bonds as well as the cluster framework in **8**$^+$ and **9** become dynamic.

(35) (a) Endres, H.; Gottstein, N.; Keller, H. J.; Martin, R.; Rodemer, W.; Steiger, W. *Z. Naturforsch., B* **1979**, *34*, 827. (b) Albano, V. G.; Chini, P.; Martinengo, S.; Sansoni, M.; Strumolo; D. *J. Chem. Soc., Dalton Trans.* **1978**, 459.

(36) Another indication for an M···M interaction is the color of the complexes. Some of the tetranuclear complexes (**8**·BF_4 and **10**·BF_4) are deeply colored (red-purple) in contrast to the pale yellow or orange color of the dinuclear complexes (**2**−**7**) and the other tetranuclear complexes (**9** and **11**). The deep color is observed only for complexes with short Rh···Rh separations. These results suggest that the color may be ascribed to an MMCT transition; further study is needed to get a conclusion, in particular, for **10**$^+$, taking into account its unusual, electronic-deficient nature. Geoffroy, G. L.; Wrighton, M. S. *Organometallic Photochemistry*; Academic: New York, 1979.

(37) See, for example: Akita, M.; Terada, M.; Moro-oka, Y. *Organometallics* **1992**, *11*, 1825. Akita, M.; Chung, M.-C.; Terada, M.; Miyauti, M.; Tanaka, M.; Moro-oka, Y. *J. Organomet. Chem.* **1998**, *565*, 49. See also references therein.

Experimental Section

General Methods. All manipulations were carried out under an inert atmosphere by using standard Schlenk tube techniques. THF, ether, hexanes, benzene, toluene (Na−K alloy), CH_2Cl_2 (P_2O_5), and EtOH ($Mg(OEt)_2$) were treated with appropriate drying agents, distilled, and stored under argon. ^1H, ^{13}C, and ^{31}P NMR spectra were recorded on Bruker AC-200 (^1H, 200 MHz; ^{31}P, 81 MHz) and JEOL EX-400 spectrometers (^{31}P, 162 MHz; ^{13}C, 100 MHz). Solvents for NMR measurements containing 0.5% TMS were dried over molecular sieves, degassed, distilled under reduced pressure, and stored under Ar. IR spectra (KBr pellets or CH_2Cl_2 solution cell) were obtained on a JASCO FT/IR 5300 spectrometer. ESI- and FD-mass spectra were recorded on a ThermoQuest Finnigan LCQ Duo and JEOL JMS-700 mass spectrometer, respectively. Complex **2**·BF_4,[3a] $PPN[Co(CO)_4]$,[38a] $PPN[Mn(CO)_5]$,[38b] and $Sn(CH{=}CH_2)_4$[15] were prepared according to the published method. Other chemicals were purchased and used as received. Chromatography was performed on alumina.

Preparation of 2a. To a THF solution (4 mL) of **2b** (63 mg, 0.077 mmol; see below) was added NBu_4·F (1 M THF solution, 7 μL, 7 μmol), and the resultant mixture was stirred for 2 h at ambient temperature. The volatiles were removed under reduced pressure, and the residue was extracted with a small amount of CH_2Cl_2 and passed through an alumina plug (eluted with THF). Concentration of the filtrate followed by addition of hexane gave **2a** as yellow crystals (58 mg, 0.077 mmol, 97% yield). ^1H NMR (CD_2Cl_2): δ_H 7.4−7.55 (12H, m, *o,p*-Ph), 7.6−7.75 (8H, m, *m*-Ph). $^{13}C\{^1H\}$ NMR (CD_2Cl_2): δ_C 129.2 (d, J_{C-P} = 11.0 Hz, *m*-Ph), 131.1 (s, *p*-Ph), 133.1 (d, J_{C-P} = 12.9 Hz, *o*-Ph), 134.0 (d, J_{C-P} = 47.7 Hz, *ipso*-Ph), 153.7 (dd, J_{C-P} = 9.2, 3.7 Hz, 3,5-pz). FD-MS: 840 (M^+). Anal. Calcd for $C_{34}H_{28}O_2N_2P_2Cl_2Rh_2$ (**2a**·CH_2Cl_2): C, 48.89; H, 3.38; N, 3.35. Found: C, 49.61; H, 3.75; N, 3.47.

Preparation of 2b−e. As a typical example, synthetic procedures for **2b** are described, and other complexes **2c−e** were prepared in a manner similar to the procedures for **2b**. To a THF solution (6 mL) of $Me_3Si{-}C{\equiv}C{-}H$ (70 μL, 0.50 mmol) cooled at −78 °C was added n-BuLi (1.57 M hexane solution, 0. 35 mL), and the resultant mixture was stirred for 20 min at the same temperature. Upon addition of **1**·BF_4 (203 mg, 0.228 mmol), vigorous gas evolution was observed. Then the cooling bath was removed and the mixture was stirred for 1.5 h. Filtration through an alumina plug followed by addition of hexanes caused precipitation of **2b** as yellow powders (142 mg, 0.173 mmol, 76% yield). ^1H NMR (CD_2Cl_2): δ_H 7.4−7.6 (12H, m, Ph), 7.65−7.8 (8H, m, Ph). $^{31}P\{^1H\}$ NMR (CD_2Cl_2): δ_P 49.7 (d, J_{P-Rh} = 142 Hz). $^{13}C\{^1H\}$ NMR (CD_2Cl_2): δ_C 128.1 (d, J = 9.1 Hz, *m*-Ph), 130.0 (s, *p*-Ph), 132.0 (d, J_{C-P} = 12.9 Hz, *o*-Ph), 133.0 (d, J_{C-P} = 45.9 Hz, *ipso*-Ph). FAB-MS: 823 (M^+). Anal. Calcd for $C_{36}H_{34}O_2N_2P_2Rh_2Si$: C, 52.57; H, 4.17; N, 3.41. Found: C, 52.68; H, 4.42; N, 3.62. **2c** (yellow crystals, 58% yield): ^1H NMR (CD_2Cl_2): δ_H 7.4−7.55 (12H, m, *o,p*-Ph), 7.65−7.8 (8H, m, *m*-Ph). $^{13}C\{^1H\}$ NMR (CD_2Cl_2): δ_C 129.1 (d, J_{C-P} = 11.0 Hz, *m*-Ph), 131.0 (s, *p*-Ph), 133.0 (d, J_{C-P} = 12.9 Hz, *o*-Ph), 134.4 (d, J_{C-P} = 45.9 Hz, *ipso*-Ph). FD-MS: 806 (M^+). Anal. Calcd for $C_{37}H_{34}O_2N_2P_2Rh_2$: C, 55.11; H, 4.25; N, 3.47. Found: C, 54.83; H, 4.35; N, 3.44. **2d** (yellow powders, 85% yield): ^1H NMR ($CDCl_3$): δ_H 7.3−7.9 (25H, m, Ph). ^{13}C NMR (owing to the low solubility in organic solvents, a satisfactory ^{13}C NMR spectrum could not be obtained). FAB-MS: 826 (M^+). Anal. Calcd for $C_{39}H_{30}O_2N_2P_2Rh_2$; C, 56.68; H, 3.66; N, 3.39. Found: C, 56.25; H, 4.02; N, 3.41. **2e** (yellow powders, 71% yield): ^1H NMR (CD_2Cl_2): δ_H 7.15 (2H, d, J_{H-P} = 8.2 Hz, tol), 7.4−7.8 (22H, m, Ph and *o*-tol). $^{13}C\{^1H\}$ NMR (CD_2Cl_2): δ_C 125.8 (s, *ipso*-tol), 129.1 (s, *m*-tol), 129.2 (d, J_{C-P} = 11.0 Hz, *m*-Ph), 131.1 (s, *p*-Ph), 131.3 (s, *o*-tol), 133.0 (d, J_{C-P} = 12.9 Hz, *o*-Ph), 134.2 (d, J_{C-P} = 45.9 Hz, *ipso*-Ph), 137.7 (s, *p*-tol). FD-MS: 840 (M^+). Anal. Calcd for $C_{40}H_{32}O_2N_2P_2Rh_2$: C, 57.16; H, 3.84; N, 3.33. Found: C, 56.42; H, 3.84; N, 2.95.

Synthesis of (μ-CH=CH_2)Rh_2(PNNP)$(CO)_2$, 3. To an ethereal solution (8 mL) of tetravinyltin (1.0 mL, 5.5 mmol) were added a catalytic amount of benzophenone (3.3 mg) and lithium wire cut into small pieces (360 mgt, 52 mmol), and the resultant suspension was stirred overnight. The supernatant was used after titration with 0.1 M aqueous HCl (2.04 M). To a THF solution (4 mL) of **1**·BF_4 (120.7 mg, 0.136 mmol) cooled at −78 °C was added $LiCH{=}CH_2$ (2.04 M, 0.3 mL, 0.6 mmol). The mixture was stirred for 2 h at the same temperature and then passed through an alumina plug. The filtrate was evaporated under reduced pressure, and trituration of the resultant oily residue by addition of hexane gave **3** (68 mg, 0.091 mmol, 76% yield) as yellow powders. Attempted purification by crystallization or chromatography induced decomposition, and **3** was characterized spectroscopically. ^1H NMR (acetone-d_6): δ_H 7.4−8.0 (m, 20H, Ph). FD-MS: 752 (M^+).

Preparation of (PNNP)$Rh_2Co(CO)_6$, 4a. Addition of **1**·BF_4 (85 mg, 0.0957 mmol) to $PPN[Co(CO)_4]$ (83 mg, 0.117 mmol) dissolved in THF (5 mL) caused gas evolution. After the mixture was stirred for 30 min, precipitates appeared. Then the mixture was concentrated under reduced pressure and passed through an alumina plug (eluted with THF). Concentration followed by addition of hexane gave **4a** as orange crystals (85 mg, 0.0949 mmol, 99% yield). ^1H NMR (CD_2Cl_2): δ_H 7.4−7.55 (m, 12H, Ph-o,p), 7.6−7.8 (m, 8H, Ph-m). $^{13}C\{^1H\}$ NMR (CD_2Cl_2): δ_C 129.5 (d, J = 11 Hz, *m*-Ph), 131.6 (s, *p*-Ph), 132.7 (d, J = 44 Hz, *ipso*-Ph), 132.9 (d, J = 13 Hz, *o*-Ph). FD-MS: 896 (M^+). Anal. Calcd for $C_{35}H_{25}O_6N_2P_2CoRh_2$: C, 46.90; H, 2.81; N; 3.13. Found: C, 46.62; H, 2.83; N, 3.15.

Preparation of (PNNP)$Rh_2Mn(CO)_7$, 4b. Treatment of **1**·BF_4 (67.0 mg, 0.0753 mmol) with $PPN[Mn(CO)_5]$ (58.0 mg, 0.0791 mmol) followed by workup as described for **4a** gave **4b** (43.0 mg, 0.0462 mmol, 61% yield) as orange crystals. ^1H NMR (CD_2Cl_2): δ_H 7.4−7.8 (m, 20H, Ph). $^{13}C\{^1H\}$ NMR (CD_2Cl_2): δ_C 129.5 (d, J = 11.0 Hz, *m*-Ph), 131.6 (s, *p*-Ph), 132.8 (d, J = 44.1 Hz, *ipso*-Ph), 132.9 (d, J = 12.9 Hz, *o*-Ph). FD-MS: 920 (M^+). Anal. Calcd for $C_{36}H_{25}O_7N_2P_2MnRh_2$: C, 46.98; H, 2.74; N, 3.04 Found: C, 46.07; H, 2.77; N, 3.10.

Preparation of [(Cy-NC)$_2$$Rh_2$(PNNP)$(CO)_2$]$BF_4$, 5. Addition of Cy-NC (20 μL, 0.16 mmol) to a THF solution of **1**·BF_4 (67.2 mg, 0.0756 mmol) caused gas evolution. After 1 h **5** (73.7 mg, 0.0715 mmol, 95% yield) was obtained as orange precipitates upon concentration and addition of Et_2O. ^1H NMR (acetone-d_6): δ_H 7.6−7.8 (m, 20H, Ph). $^{13}C\{^1H\}$ NMR (acetone-d_6): δ_C 130.2 (t, J = 11.9 Hz, Ph), 131.2 (d, J = 44.1 Hz, Ph), 131.4 (t, J = 55.2 Hz, Ph), 132.5 (d, J = 5.5 Hz, Ph), 133.2 (d, J = 12.9 Hz, Ph), 133.7 (d, J = 12.9 Hz, Ph). ESI-MS: 943 (M^+). Anal. Calcd for $C_{45}H_{47}O_2N_4P_2BF_4Rh_2$: C, 52.45; H, 4.60; N, 5.44. Found: C, 52.19; H, 5.05; N, 5.18.

Preparation of [(μ-SMe_2)Rh_2(PNNP)$(CO)_2$]BF_4, 6. Reaction of **1**·BF_4 (74 mg, 0.0826 mmol) with SMe_2 (7 μL, 0.094 mmol) in acetone (3 mL) gave **6** (47.3 mg, 0.054 mmol, 65% yield; brown solid) after removal of the volatiles under reduced pressure followed by crystallization from CH_2Cl_2−Et_2O. ^1H NMR (acetone-d_6): δ_H 7.5−7.9 (m, 20H, Ph). $^{13}C\{^1H\}$ NMR (acetone-d_6): δ_H 130.0 (dd, J = 12.5 Hz, 1.4 Hz, *m*-Ph), 131.9 (dd, J = 52.1 Hz, 2.0 Hz, *ipso*-Ph), 132.4 (t, J = 1.1 Hz, *p*-Ph), 133.4 (dd, J = 12.3 Hz, 1.1 Hz, *o*-Ph). ESI-MS: 788 (M^+). Anal. Calcd for $C_{33}H_{31}O_2N_2P_2SBF_4Rh_2$: C, 45.34; H, 3.57; N, 3.20; S, 3.67. Found: C, 45.35; H, 4.00; N, 3.17; S, 3.31.

Preparation of [(μ-Et-C≡C-Et)Rh_2(PNNP)$(CO)_2$]BF_4, 7. An acetone solution (5 mL) of **1**·BF_4 (92.0 mg, 0.103 mmol) and 3-hexyne (15 μL, 0.132 mmol) was refluxed for 1 h. The color of the solution changed from yellow to red. Removal of the volatiles under reduced pressure left an oily red residue,

(38) (a) Ruff, J. K.; Schlientz. *Inorg. Synth.* **1974**, *15*, 84. (b) Duffy, D. N.; Nicholson, B. K. *J. Organomet. Chem.* **1979**, *164*, 227.

which was characterized as **7**. Attempted purification of hexane by crystallization and chromatography resulted in decomposition. **7**: ^{1}H NMR (200 MHz, acetone-d_6): δ_H 7.5−7.9 (m, 20H, Ph). ^{13}C{^{1}H} NMR (acetone-d_6): δ_C 130.4 (d, J = 11.0 Hz, *m*-Ph), 132.8 (s, *p*-Ph), 133.6 (d, J = 11.0 Hz, *o*-Ph).

Preparation of 8a·BF$_4$. Addition of **1**·BF$_4$ (45.8 mg, 0.051 mmol) to a CH_2Cl_2 solution (3 mL) of **2a** (37.0 mg, 0.049 mmol) cooled in an ice bath caused an immediate color change to deep red. The resultant mixture was stirred for 1 h at 0 °C and then concentrated under reduced pressure at 0 °C. Addition of ether gave red-brown precipitates, **8a**·BF$_4$ (75 mg, 0.048 mmol, 97% yield), which were collected on a glass frit and dried in vacuo. ^{1}H NMR (CD_2Cl_2): δ_H 7.3−7.7 (m, 40H, Ph). ^{13}C{^{1}H} NMR (CD_2Cl_2): δ_C 129.2 (d, J_{C-P} = 12.9 Hz, *m*-Ph), 131.6 (s, *p*-Ph), 132.7 (d, J_{C-P} = 12.9 Hz, *o*-Ph), 133.5 (d, J_{C-P} = 45.3 Hz, *ipso*-Ph). Despite several attempts an analytically pure sample could not be obtained.

Preparation of 8b−e·BF$_4$. As a typical example, synthetic procedures for **8e**·BF$_4$ are described, and other complexes were prepared in a manner similar to the procedures for **8e**·BF$_4$ unless otherwise stated. Addition of *p*-tol-C≡C−H (22 μL, 0.156 mmol) to an acetone solution (5 mL) of **2**·BF$_4$ (151 mg, 0.170 mmol) caused an immediate color change to deep red. The mixture was stirred for 1 h and then concentrated under reduced pressure. Addition of ether gave deep red precipitates, which were collected by filtration. The obtained deep red powder was dissolved in a minimum amount of CH_2Cl_2 and subjected to alumina column chromatography. Elution with CH_2Cl_2 gave a yellow band and then a deep red band. Collection of the deep red band followed by concentration, addition of toluene, and cooling at −20 °C gave **8e**·BF$_4$ as deep red crystals (80.0 mg, 0.048 mmol, 56% yield). **8e**·BF$_4$: ^{1}H NMR (CD_2Cl_2): δ_H 6.98 (d, J = 8.0 Hz, 2H, *m*-tol), 7.3−7.7 (m, 40H, Ph), 7.81 (d, J = 8.0 Hz, 2H, *o*-tol). ^{13}C{^{1}H} NMR (CD_2Cl_2): δ_C 125.2 (s, *ipso*-tol), 129.1 (s, *m*-tol), 129.3 (d, J_{C-P} = 10.9 Hz, *m*-Ph), 131.5 (s, *p*-Ph), 132.7 (d, J_{C-P} = 12.9 Hz, *o*-Ph), 133.2 (d, J_{C-P} = 49.6 Hz, *ipso*-Ph), 136.5 (s, *o*-tol), 141.6 (s, *p*-tol). ESI-MS: 1565 (M^+ for **5a**$^+$). Anal. Calcd for $C_{78}H_{65}O_4N_4P_4BF_4Rh_4$ (**8e**·BF$_4$·toluene): C, 53.73; H, 3.70; N, 3.21. Found: C, 53.44; H, 3.84; N, 3.18. The BPh$_4$ salt subjected to X-ray crystallography was obtained by metathesis of **8e**·BF$_4$ with NaBPh$_4$ in acetone followed by extraction with CH_2Cl_2 and crystallization by addition of hexane. **8b**·BF$_4$: ^{1}H NMR (CD_2Cl_2): δ_H 7.3−7.8 (m, 40H, Ph). ^{13}C{^{1}H} NMR (CD_2Cl_2): δ_C 129.2 (d, J = 10.9 Hz, *m*-Ph), 131.5 (s, *p*-Ph), 132.5 (d, J_{C-P} = 12.9 Hz, *o*-Ph), 132.7 (d, J_{C-P} = 47.7 Hz, *ipso*-Ph). ESI-MS: 1548 (M^+). Attempted purification caused partial desilylation to give a mixture containing **8a**·BF$_4$. **8c**·BF$_4$: ^{1}H NMR (CD_2Cl_2): δ_H 7.3−7.8 (m, 40H, Ph). ^{13}C{^{1}H} NMR (CD_2Cl_2): δ_C 129.4 (d, J_{C-P} = 11.0 Hz, *m*-Ph), 131.6 (s, *p*-Ph), 132.7 (d, J_{C-P} = 10.9 Hz, *o*-Ph), 133.1 (d, J_{C-P} = 53.2 Hz, *ipso*-Ph). ESI-MS: 1532 (M^+). Anal. Calcd for $C_{75}H_{67}O_4N_4P_4BF_4Rh_4$ (**8c**·BF$_4$·toluene): C, 52.66; H, 3.95; N, 3.28. Found: C, 53.18; H, 4.30; N, 3.15. **8d**·BF$_4$: ^{1}H NMR (acetone-d_6): δ_H 7.28 (t, J = 7.6 Hz, 2H, *m*-C_2Ph), 7.4−7.8 (m, 41H, PPh and *p*-C_2Ph), 8.08 (d, J = 7.3 Hz, 2H, *o*-C_2Ph). ^{13}C{^{1}H} NMR (acetone-d_6): δ_C 128.9 (s, *ipso*-C_2Ph), 128.9 (s, *m*-C_2Ph), 129.9 (d, J_{C-P} = 10.9 Hz, *m*-Ph), 131.1 (s, *p*-C_2Ph), 132.2 (s, *p*-Ph), 133.3 (d, J_{C-P} = 12.9 Hz, *o*-Ph), 133.9 (d, J_{C-P} = 53.3 Hz, *ipso*-Ph), 137.1 (s, *o*-C_2Ph). ESI-MS: 1554 (M^{+2}). Anal. Calcd for $C_{70.5}H_{56}O_4N_4P_4BClF_4Rh_4$ [**8d**·BF$_4$·$(CH_2Cl_2)_{0.5}$]: C, 50.37; H, 3.36; N, 3.33. Found: C, 50.20; H, 3.82; N, 3.35.

Preparation of 9. Complex **8a**·BF$_4$ (224 mg, 0.137 mmol) was dissolved in a minimum amount of CH_2Cl_2 and subjected to alumina column chromatography. Elution with CH_2Cl_2 gave a yellow-orange band, from which **9**·BF$_4$ (120 mg, 0.081 mmol, 59% yield) was isolated as a yellow-orange powder after addition of hexane. ^{1}H NMR (CD_2Cl_2): δ_H 7.3−7.9 (m, 20H, Ph). ^{13}C{^{1}H} NMR (CD_2Cl_2): δ_C 128.9 (d, J_{C-P} = 9.2 Hz, *m*-Ph), 130.6 (s, *p*-Ph), 133.3 (d, J_{C-P} = 12.9 Hz, *o*-Ph), 135.1 (d, J_{C-P} = 44.0 Hz, *ipso*-Ph). FAB-MS: 1473 (M^+ for **9**). Anal. Calcd for $C_{63.5}H_{51}O_4N_4P_4ClRh_4$ [**9**·$(CH_2Cl_2)_{0.5}$]: C, 50.67; H, 3.42; N, 3.72. Found: C, 50.44; H, 3.64; N, 3.69.

Preparation of 10·BF$_4$. To a THF solution (20 mL) of $HSiEt_3$ (40 μL, 0.25 mmol) was added **1**·BF$_4$ (258 mg, 0.272 mmol), and the resultant mixture was stirred at ambient temperature until gas evolution ceased (ca. 1.5 h). The supernatant was removed via a cannula, and the remaining purple precipitate was washed with a minimum amount of THF and dried under reduced pressure. **10**·BF$_4$ (119 mg, 0.078 mmol, 57% yield) was obtained as a deep purple powder. Crystallization from CH_2Cl_2−hexane afforded deep purple plates. Complex **10**·BF$_4$: ^{1}H NMR (CD_2Cl_2): δ_H 7.4−7.7 (m, 40H; Ph). ^{13}C{^{1}H} NMR (CD_2Cl_2): δ_C 133.0 (d, J_{C-P} = 50 Hz, *ipso*-Ph), 132.9 (d, J_{C-P} = 13 Hz, *o*-Ph), 131.7 (s, *p*-Ph), 129.5 (d, J_{C-P} = 13 Hz, *m*-Ph). ESI-MS: *m/z*: 1451 [M^+ for the cationic part (**10**$^+$)]. Anal. Calcd for $C_{62.5}H_{52}O_4N_4P_4BF_4ClRh_4$ [**10**·BF$_4$·$(CH_2Cl_2)_{0.5}$]: C, 47.48; H, 3.32; N, 3.54. Found: C, 47.09; H, 3.29; N, 3.54. **10**·BPh$_4$: To a THF−CH_2Cl_2 solution (1:1; 10 mL) of **10**·BF$_4$ (100 mg, 0.065 mmol) was added a THF−CH_2Cl_2 solution (1:1; 3 mL) of NaBPh$_4$ (42 mg, 0.12 mmol), and the resultant mixture was stirred for 20 min. After removal of the volatiles under reduced pressure the residue was extracted with CH_2Cl_2, and addition of hexane gave deep purple crystals of the BPh$_4$ salts (105 mg, 0.059 mmol, 91% yield).

Preparation of (μ_4-O)Rh$_4$(PNNP)$_2$(CO)$_4$, 11. To an acetone solution (3 mL) of **1**·BF$_4$ (104.1 mg, 0.117 mmol) was added water (2 μL, 0.11 mmol) and NEt_3 (0.016 mL, 0.11 mmol), and the resultant mixture was stirred for 2 h. Orange precipitates formed, **11** (55.0 mg, 0.038 mmol, 32% yield), were collected on a glass frit and dried in vacuo. **11** was also obtained in 34% yield by treatment of **1**·BF$_4$ with a THF solution of KOH (14 mg/4 mL). ^{1}H NMR (CD_2Cl_2): δ_H 7.3−8.0 (m, 20H, Ph). Anal. Calcd for $C_{63}H_{52}O_5N_4P_4Cl_2Rh_4$ (**11**·CH_2Cl_2): C, 48.77; H, 3.38; N, 3.61. Found: C, 48.82; H, 3.27; N, 3.71.

X-ray Crystallography. Single crystals were obtained by recrystallization from CH_2Cl_2−hexane except for **2a** (from benzene) and mounted on glass fibers. Diffraction measurements were made on a Rigaku RAXIS IV imaging plate area detector with Mo Kα radiation (λ = 0.71069 Å) at −60 °C. Indexing was performed from two oscillation images, which were exposed for 5 min. The crystal-to-detector distance was 110 mm ($2\theta_{max}$ = 55°). In the reduction of data, Lorentz and polarization corrections and empirical absorption corrections were made.[39] Crystallographic data and results of structure refinements are listed in Table 5.

The structural analysis was performed on an IRIS O2 computer using the teXsan structure solving program system obtained from the Rigaku Corp., Tokyo, Japan.[40] Neutral scattering factors were obtained from the standard source.[41]

The structures were solved by a combination of the direct methods (SHELXS-86)[42] and Fourier synthesis (DIRDIF94).[43] Least-squares refinements were carried out using SHELXL-97 [42] (refined on F^2) linked to teXsan. All non-hydrogen atoms were refined anisotropically. Hydrogen atoms were fixed at the calculated positions unless otherwise stated. **2a**: The C_2H

(39) Higashi, T. *Program for Absorption Correction*, Rigaku Corp.: Tokyo, Japan, 1995.

(40) *teXsan; Crystal Structure Analysis Package,* ver. 1. 11; Rigaku Corp., Tokyo, Japan, 2000.

(41) *International Tables for X-ray Crystallography*; Kynoch Press: Birmingham, 1975; Vol. 4.

(42) (a) Sheldrick, G. M. *SHELXS-86: Program for crystal structure determination*; University of Göttingen: Göttingen, Germany, 1986. (b) Sheldrick, G. M. *SHELXL-97: Program for crystal structure refinement*; University of Göttingen: Göttingen, Germany, 1997.

(43) Beurskens, P. T.; Admiraal, G.; Beurskens, G.; Bosman, W. P.; Garcia-Granda, S.; Gould, R. O.; Smits, J. M. M.; Smykalla, C. *The DIRDIF program system, Technical Report of the Crystallography Laboratory*; University of Nijmegen: Nijmegen, The Netherland, 1992.

Table 5. Crystallographic Data

	2a	**2b**	**2c**	**2d**	**2e**
solvate	$(C_6H_6)_{1.4}$	H_2O			
formula	$C_{33}H_{26}N_2O_2P_2Rh_2$	$C_{36}H_{35}N_2O_3SiP_2Rh_2$	$C_{37}H_{34}N_2O_2P_2Rh_2$	$C_{39}H_{30}N_2O_2P_2Rh_2$	$C_{40}H_{32}N_2O_2P_2Rh_2$
fw	750.32	839.51	806.42	826.41	840.44
cryst syst	monoclinic	triclinic	triclinic	monoclinic	triclinic
space group	$P2_1/c$	$P\bar{1}$	$P\bar{1}$	Cc	$P\bar{1}$
a/Å	11.9921(4)	17.660(4)	12.8265(11)	22.5676(10)	12.8840(9)
b/Å	14.4141(8)	19.519(4)	13.777(2)	8.5213(3)	12.8835(8)
c/Å	17.4658(9)	11.385(2)	12.6402(14)	17.8092(5)	12.7042(7)
α/deg	90	98.981(15)	104.166(3)	90	104.022(4)
β/deg	91.523(3)	89.908(7)	113.280(5)	97.387(2)	108.780(3)
γ/deg	90	65.347(4)	70.131(2)	90	65.142(2)
V/Å^3	3018.0(2)	3513.4(13)	1913.8(4)	3396.4(2)	1797.4(2)
Z	4	4	2	4	2
d_{calcd}/g·cm^{-3}	1.651	1.587	1.399	1.616	1.553
μ/mm^{-1}	1.233	1.102	0.977	1.104	1.044
no. of reflns collected	23 371	21 956	7924	13 623	14 069
no. of variables	374	825	407	424	433
R1 for data with $I > 2\sigma(I)$	0.0311 (for 5768 data)	0.1033 (for 8728 data)	0.0710 (for 4890 data)	0.0325 (for 3568 data)	0.0431 (for 6991 data)
wR2	0.0960 (for all 6234 data)	0.2692 (for all 13506 data)	0.2193 (for all 7924 data)	0.0978 (for all 3849 data)	0.1450 (for all 7401 data)

	4a	**4b**	**8e**·BPh_4	**9**	**10**·BPh_4
solvate	CH_2Cl_2	$(CH_2Cl_2)_2$			$(CH_2Cl_2)_2$·(hexane)$_{1/2}$
formula	$C_{36}H_{27}N_2O_6P_2Cl_2CoRh_2$	$C_{38}H_{29}N_2O_7Cl_4P_2MnRh_2$	$C_{95}H_{77}BN_4O_4P_4Rh_4$	$C_{64}H_{50}N_4O_4P_4Rh_4$	$C_{91}H_{82}BN_4O_4P_4Cl_4Rh_4$
fw	981.19	1090.13	1884.94	1474.64	1983.74
cryst syst	triclinic	triclinic	monoclinic	monoclinic	triclinic
space group	$P\bar{1}$	$P\bar{1}$	$P2_1/a$	$P2_1/c$	$P\bar{1}$
a/Å	11.9167(16)	13.14410(10)	17.9746(3)	22.608(3)	17.8753(14)
b/Å	14.4746(19)	14.5146(4)	27.7046(6)	19.320(3)	18.8768(13)
c/Å	11.6363(13)	13.0817(3)	16.6001(3)	14.927(4)	13.7743(10)
α/deg	98.247(9)	96.1360(10)	90	90	103.703(3)
β/deg	112.296(8)	115.0510(10)	90.8460(10)	110.979(4)	97.179(5)
γ/deg	88.002(3)	68.505(2)	90	90	105.748(5)
V/Å^3	1837.5(4)	2100.27(8)	8265.6(3)	6087(1)	4256.1(6)
Z	2	2	4	4	2
d_{calcd}/g·cm^{-3}	1.773	1.724	1.515	1.609	1.548
μ/mm^{-1}	1.614	1.453	0.917	1.218	1.016
no. of reflns collected	13 327	16 592	57 193	48 675	16 104
no. of variables	460	483	1010	721	968
R1 for data with $I > 2\sigma(I)$	0.0725 (for 6774 data)	0.0602 (for 6950 data)	0.0431 (for 11 068 data)	0.0680 (for 8137 data)	0.0664 (for 11 879 data)
wR2	0.2215 (for all 7460 data)	0.1769 (for all 8644 data)	0.1270 (for all 17 789 data)	0.1926 (for all 13 846 data)	0.1792 (for all 16 104 data)

Complex **11**

formula	$C_{71}H_{59}N_4O_5P_4Rh_4$	V/Å^3	3248.2(7)
fw	1583.74	Z	2
cryst syst	triclinic	d_{calcd}/g·cm^{-3}	1.619
space group	$P\bar{1}$	μ/mm^{-1}	1.151
a/Å	14.2214(15)	no. of reflns collected	12 182
b/Å	21.678(2)	no. of variables	793
c/Å	12.3153(16)	R1 for data	0.0785
α/deg	105.141(5)	with $I > 2\sigma(I)$	(for 7331 data)
β/deg	107.050(10)	wR2	0.2366
γ/deg	105.634(8)		(for all 12 182 data)

hydrogen atom was refined isotropically. **2b**: Hydrogen atoms attached to the water solvates were not included in the refinement. **2e** and **8e**·BPh_4: Methyl hydrogen atoms were refined with riding models. **4b**: CH_2Cl_2 solvate molecules were refined isotropically, and one of them was found to be disordered (Cl2−C61:Cl2a−C61a = 0.688:0.312). Hydrogen atoms attached to the CH_2Cl_2 solvate molecules were not included in the refinement. **10**·BPh_4: The disordered CH_2Cl_2 molecule was refined taking into account the minor component (Cl4:Cl4a = 0.52:0.48), and the highly disordered terminal methyl group of the hexane solvate could not be located and was not included in the refinement. The μ_4-hydride atom (H1) was refined isotropically, but the hydrogen included the PNNP and BPh_4 moieties were fixed at the calculated positions and not refined. The hydrogen atoms of the solvates are not included in the refinement.

Acknowledgment. We are grateful to the Ministry of Education, Culture, Sports, Science and Technology of the Japanese Government (Grant-in-Aid for Scientific Research on Priority Area, No. 16033219) and the Japan Society for Promotion of Science and Technology (Grant-in-Aid for Scientific Research (B): No. 15350032) for financial support of this research. A Monbukagakusho scholarship for C.D. from the Japanese Government is also gratefully acknowledged.

Supporting Information Available: Crystallographic results. This material is available free of charge via the Internet at http://pubs.acs.org.

OM049427V